AD NUMBER

AD281819

NEW LIMITATION CHANGE

TO

Approved for public release, distribution unlimited

FROM

Distribution authorized to U.S. Gov't. agencies and their contractors; Administrative/Operational Use; MAR 1962. Other requests shall be referred to U.S. Army Signal Research and Development Laboratory, Fort Monmouth, NJ.

AUTHORITY

USAEC ltr, 25 Apr 1973

AI–7330
COPY

FLAME HEATED THERMIONIC CONVERTER RESEARCH

Report No. 3
Third Quarterly Report
(1 January 1962 to 31 March 1962)
Contract No. DA–36–039 SC–88982

Department of the Army Task No. 3A99–09–002–04
U. S. Army Signal Research & Development Laboratory,
Fort Monmouth, New Jersey

ATOMICS INTERNATIONAL
A DIVISION OF NORTH AMERICAN AVIATION, INC.

AI-7330

FLAME HEATED THERMIONIC CONVERTER RESEARCH

Report No. 3
Third Quarterly Report
(1 January 1962 to 31 March 1962)

By:
W. R. MARTINI
R. L. McKISSON
E. V. CLARK

Power Sources Division Technical Guidelines for PR & C
No. 61-ELP/D-4623 dated 23 December 1960

Department of the Army Task No. 3A99-09-002-04

Object: To develop the technology required for portable flame heated thermionic power sources.

ATOMICS INTERNATIONAL
A DIVISION OF NORTH AMERICAN AVIATION, INC.
P.O. BOX 309 CANOGA PARK, CALIFORNIA

CONTRACT: DA-36-039 SC 88982
ISSUED: [illegible] 1962

CONTENTS

	Page
Purpose	1
Program Outline	2
Abstract	4
Publications, Lectures, Reports, and Conferences	5
Technical Progress	6
Task A - Thermionic Converter Development	6
Phase 1 - Diode Construction	6
Examination of the 150 w(e) Diode	6
Construction of Fuel-Fired Demonstration Diodes	8
Phase 2 - Diode Performance Characteristics	9
Triggered Diode	11
Diode Switching	17
Task B - Heat Source Development	17
Phase 1 - Aspirated Burner Development	17
Phase 2 - Fan-Powered Burner Development	17
High Efficiency Heater Development	17
Demonstration Diode Heater Development	19
Runs DD-1 to DD-3	21
Runs DD-4 to DD-8	23
Runs DD-9 to DD-12	23
Runs DD-13 to DD-16	25
Runs DD-17 to DD-20	29
Runs DD-21 to DD-27	29
Comparison of All Runs	31
Phase 3 - Temperature Control	34
Phase 4 - System Construction and Operation	35
Phase 5 - System Design and Analysis	37
Thermodynamic Relationships	37
Heat Exchanger Operation, Premixed Air and Fuel	38
Heat Exchanger Operation, Fuel Injection	38
Theoretical Overall Efficiency	41
Heat Exchanger Limitations	42

CONTENTS

Page

Task C - Materials Development and Evaluation 45
Phase 1 - Protection of Molybdenum 45
Summary of Durak-B Data 45
Supplemental Protection With a Glaze 49
Protection From Flame Components 49
Metallographic Examination 49
Phase 2 - Corrosion of Silicon Carbide 53
Phase 3 - Gas Permeation 53
Phase 4 - Welding of Molybdenum 53
Conclusions 56
Program for Next Quarter 57
Key Personnel Assigned to Project 58
Nomenclature 59
References 60

TABLES

I. Results of High Efficiency Burner Experiment No. 1 18
II. Results of Runs DD-1 to DD-3 20
III. Results of Runs DD-4 to DD-8 22
IV. Results of Runs DD-9 to DD-12 26
V. Results of Runs DD-13 to DD-16 27
VI. Results of Runs DD-17 to DD-20 28
VII. Results of Runs DD-21 to DD-27 30
VIII. Selected Fuel Properties 36
IX. Maximum Heat Exchanger Efficiency With Continuous Fuel Injection (T_e = 1500°C) 41
X. Summary of Corrosion Experiments on Durak-B Coated Molybdenum Samples 48
XI. Summary of SiC Tests 52

FIGURES

Page

1. Detail Examination of 150 w(e) Diode 6
2. Shattered, but Functioning, Sapphire Spacer
   a. Broken Spacer in Collector Assembly 7
   b. Scars on Emitter Assembly 7
3. Crack Through Ni-Mo Braze in 150 w(e) Diode 8
4. Second Demonstration Flame-Heated Thermionic Diode 10
5. 150 w(e) Diode Operating History 11
6. Triggered Diode Power Inversion System 12
7. Typical Bi-Stable Diode Volt-Ampere Curve 12
8. 150 w(e) Diode Volt-Ampere Curves 14
9. Operating Regions for Triggered Diode Power Inversion System 15
10. Observations on Ignition Point as a Function of Emitter Temperature 16
11. High-Efficiency Heater Experiment No. 1 18
12. Experimental Setup for Heater Experiment Runs DD-1 to DD-3 20
13. Experimental Setup and Temperature Distribution for Heater Experiment Runs DD-4 to DD-8 22
14. Test of Second Demonstration Diode Heater 24
15. Test Furnace for Second Demonstration Diode Heater 24
16. Insulating Flow Baffle and Combustion Crucible 24
17. Experimental Setup and Temperature Distribution for Heater Experiment Runs DD-9 to DD-12 26
18. Temperature Distribution for Heater Experiment Runs DD-13 to DD-16 27
19. Temperature Distribution for Heater Experiment Runs DD-17 to DD-20 28
20. Temperature Distribution for Heater Experiment Runs DD-21 to DD-27 30
21. Combustion Chamber Temperature vs Heat Input (Runs DD-1 to DD-27) 32
22. Heating Efficiency vs Combustion Chamber Temperature (Runs DD-1 to DD-27) 32
23. Heat Flux vs Combustion Chamber Temperature (Runs DD-1 to DD-27) 33
24. Air Supply Pressure vs Combustion Chamber Temperature (Runs DD-1 to DD-27) 33

FIGURES

Page

25. Pressure-Temperature Relationship for Water-Filled Constant Temperature Tubes 35
26. Maximum Heating Efficiency for Various Fuels (T_e = 1500°C, 10% Excess Air, Perfect Flame-Emitter Heat Transfer) 36
27. Maximum Heating Efficiency for Gasoline 39
28. Emission-Limited Efficiencies for the Cesium Thermionic Converter 40
29. Maximum Overall Efficiencies for Flame-Heated Thermionic Converter Systems (Gasoline Fueled) 40
30. Design Chart for Regular Gasoline Fueled Diode Heaters (Q_I = 0) 43
31. Protection Life of $MoSi_2$ Coatings, Exposure in Air 44
32. Protection Life of Durak-B Coatings, Exposure in Air 46
33. Protection Life of Durak-B Coatings in Flame Components 47
34. Summary of $MoSi_2$ Coating Behavior After Air Exposures 50
35. Photomicrograph of Successful Mo-Mo End Cap Weld 54
36. Mo-to-Mo Welds 54

PURPOSE

The purpose of the procurement is to investigate the various problems encountered in the design and construction of thermionic generators capable of producing from 5 to 200 w of power. These problems cover:

1) The selection of suitable materials for thermionic diode envelopes and heat ducts, where high temperatures and corrosive gases are encountered.

2) The design of a fossil-fuel burner, capable of providing the required temperatures and heating rates.

3) The establishment of design parameters for thermionic generators of various power levels from 5 to 200 w.

4) The construction of a sample generator, rated at 100 w output, to demonstrate the feasibility of the design approach.

PROGRAM OUTLINE

TASK A - THERMIONIC CONVERTER DEVELOPMENT

1. Construct converters for testing, with or without protective coating, as required.
2. Study the basic performance characteristics of diodes designed for use in the 100-w Thermionic Generator program.
3. Using the same equipment as for Number 2, operate diodes for up to 1000 hr to determine lifetime characteristics for the diode itself.

TASK B - HEAT SOURCE DEVELOPMENT

1. Develop aspirated regenerative burners for propane and for gasoline.
2. Develop a fan-powered regenerator burner assembly for gasoline fuel.
3. Develop temperature controls for emitter, collector, cesium reservoir, and fuel injector.
4. Construct and operate the 100-w thermionic generator prototypes, including the integration of combustion chamber, converters, electrical conversion,* and control equipment.
5. Design converters for 5 to 200 w power levels at 6,12, and 24 v dc, and analyze performance expectations.
6. Perform environmental tests on thermionic generator prototypes.

TASK C - MATERIALS DEVELOPMENT AND EVALUATION

1. Perform corrosion tests on molybdenum and molybdenum alloys coated with molybdenum disilicide in air and in flame component environments at thermionic temperatures.
2. Perform corrosion tests on silicon carbide base refractories and other related materials in oxidizing, neutral, and reducing flames at material temperatures up to 1700°C.
3. Determine permeability of gases through molybdenum or molybdenum alloy thimbles coated with a superior anticorrosion coating, as determined by Number 1 above. Identify the gases diffusing through at thermionic temperatures.

*Solid state electrical-electrical conversion development is excluded.

ABSTRACT

TASK – THERMIONIC CONVERTER DEVELOPMENT

Parts for four flame-heated diodes have been fabricated, and are ready for assembly.

The cesium leak in the 150 w(e) electrically-heated diode was found to be chiefly through a crack in the alumina of the seal. The sapphire spacers were found to prevent shorting between emitter and collector, even though shattered by thermal stress. Before the cesium was depleted, some information was obtained, defining the operating conditions needed for a triggered diode power inversion system.

TASK B – HEAT SOURCE DEVELOPMENT

Although some work was done on a high efficiency burner experiment, the chief effort was in the development of a heater for the demonstration diode. A combustion chamber temperature of 1450°C was attained, along with a heat flux of 28 w/cm^2. An analysis of heat sources, from the standpoint of thermodynamics and heat transfer, showed the eventual necessity of using a heater employing fuel injection in combination with a high efficiency heat exchanger.

TASK C – MATERIALS DEVELOPMENT AND EVALUATION

Testing of Durak-B coating for molybdenum metal continued. We now realize that the coating fails due to depletion of silicon, either by diffusion into the molybdenum metal or by evaporation off the surface. Also, it appears that the silica glass layer protecting the Durak-B changes to crystobalite around 1300°C. Cracks in the crystobalite do not heal over as readily, and cause the wire to fail more easily at this point than at a much higher temperature (1700°C) where silica glass is the stable phase.

Tests on flame corrosion of silicon carbide bodies showed that KT silicon carbide was much better than any other type. Nevertheless, corrosion became rapid over 1700°C.

Capsules were successfully fabricated by welding, so that the gas permeability of hot Durak-B coated molybdenum could be carried out. This required the development of a new welding technique.

PUBLICATIONS, LECTURES, REPORTS, AND CONFERENCES

W. R. Martini has prepared a paper, entitled "Design Considerations for Gasoline Powered Thermionic Generators," to be presented at the Sixteenth Annual Power Sources Conference, sponsored by the Power Sources Division of the U. S. Army Signal Research and Development Laboratory, to be held on May 22-24, 1962, at Atlantic City, New Jersey.

Three papers have been prepared for presentation at the Symposium on Thermionic Power Conversion, May 14-17, 1962, at Colorado Springs, Colorado. They are:

1) "Theoretical Calculation of the Thermal Conductivity of Cesium Vapor at Thermionic Temperatures," by W. R. Martini,

2) "Progress in the Development of Flame-Heated Thermionic Power Sources," by W. R. Martini and R. L. McKisson,

3) "Emitter Corrosion in Thermionic Converters," by R. L. McKisson.

TECHNICAL PROGRESS

TASK A – THERMIONIC CONVERTER DEVELOPMENT

Phase 1 – Diode Construction

During this quarter, work under Phase 1 has been concerned with, (1) examination of the 150-w electrically heated diode, after it had failed and could not be repaired, and (2) construction of four flame-heated diodes, for the purpose of submitting a sample product.

Examination of the 150 w(e) Diode

The cesium leak in the 150-w electrically heated converter[1] was found to be virtually impossible to repair. The unit was therefore disassembled for detailed examination of the critical regions.

As a first step in the disassembly of the diode, the cesium reservoir was cut off, to permit evacuation and a helium leak-check of the unit. Leaks were found in the ceramic insulator and in the nickel braze joint (See Figure 1). The diode was then carefully disassembled in the following manner:

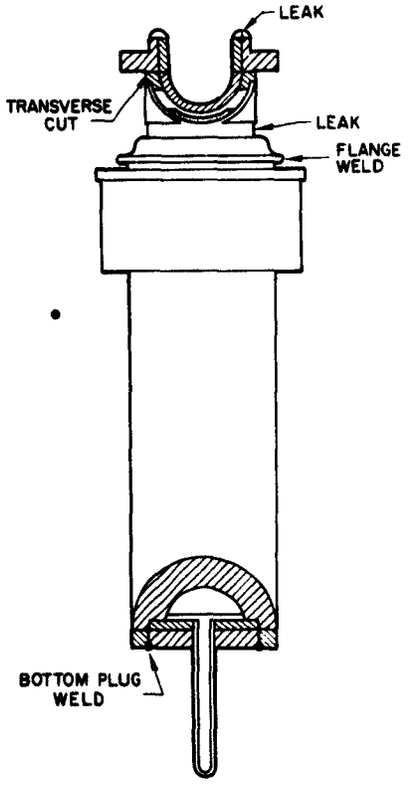

Figure 1. Detail Examination of 150 w(e) Diode

1) The bottom plug weld was machined away, and the plug removed;

2) The flange weld on the lip of the ceramic-metal seal was ground off, and the cathode (with the ceramic-metal seal) was withdrawn from the anode;

3) The nickel braze joint with the top edges of the cathode and ceramic-metal seal was severed by a transverse cut with a silicon carbide wheel.

The parts were next examined for visual defects. The first important discovery was the fracture of the sapphire buttons which prevented accidental shorting of the diode at the unsupported end of the cathode. A typical broken button is shown in Figure 2a. Matching scars on the cathode

2414-1819 D

a. Broken Spacer in Collector Assembly

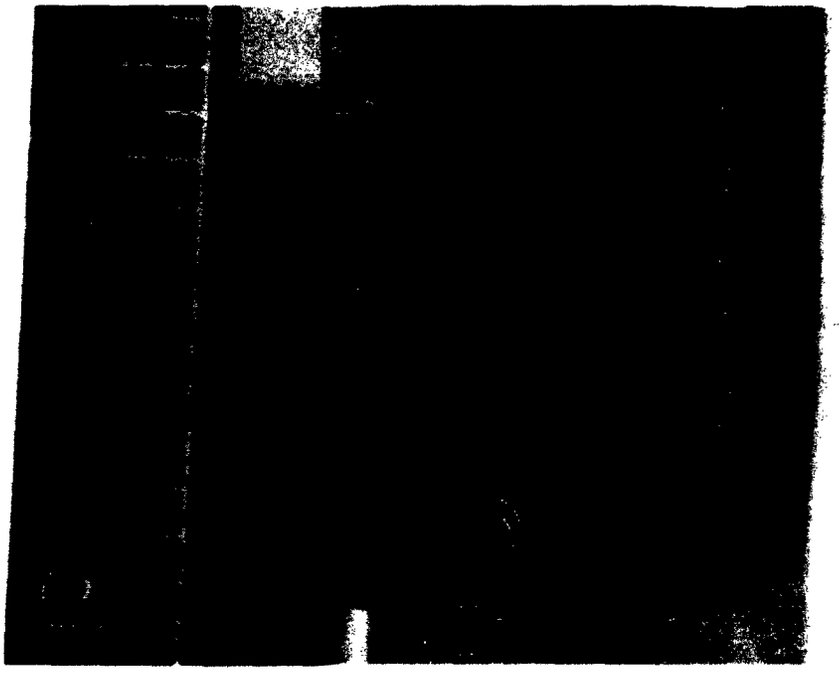

2414-1819 B

b. Scars on Emitter Assembly

Figure 2. Shattered, but Functioning, Sapphire Spacer

are shown in Figure 2b. Further examination revealed that the sapphire buttons had been installed improperly, due to the lack of preload in the threads of the backup plugs. This lack allowed the initial annular clearance to decrease during welding. Then, on rapid heatup of the diode, the emitter could expand out against the spacers with sufficient force to cause them to shatter.

The leak in the ceramic-metal seal was caused by a longitudinal crack, the full length of the ceramic piece. Typical discoloration tracking was seen in this region on the inside of the seal (the crack was indistinguishable in the outside glaze, and an attempt to obtain a picture of the crack was unsuccessful, due to the hardness of alumina). It appears that the seal failed due to overheating. More attention must be paid to seals in the future, especially when high-temperature operation is required.

The nickel braze joint was sectioned and examined microscopically in the leak area. Figure 3 shows the propagation of a crack starting at the molybdenum-nickel interface and extending to the outside surface.

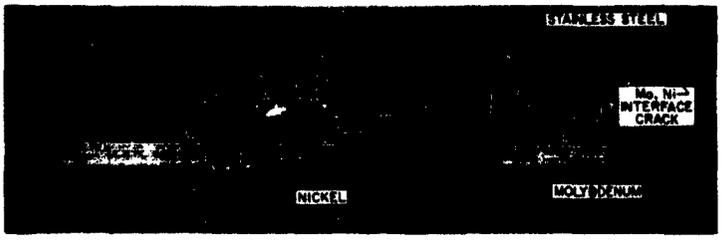

Figure 3. Crack Through Ni-Mo Braze in 150 w(e) Diode

As is reported in the literature,[2] nickel brazing of molybdenum leaves a brittle interface. Thus, thermal stresses on the top cathode joint cracked this braze, because the thick section of nickel prevented strain relief. The crack then propagated along grain boundaries, forming a leak path for cesium.

All other parts of the diode were quite normal in appearance. Microscopic examination of the copper braze in the ceramic-metal seal revealed no evidence of attack by the cesium.

Construction of Fuel-Fired Demonstration Diodes

To illustrate present thinking on the design of fuel-fired thermionic converters, four demonstration units are now under construction. Basically, the

units are internally-fired, parallel-plate configuration, using a sapphire part to maintain the interelectrode spacing.

Internal heating was chosen to decrease the severe heat losses experienced in the first flame-heated unit, and the parallel-plate diode geometry was retained for simplicity. Since it has been virtually impossible to predict exact temperature behavior in these converters, a method was sought for obtaining and holding a fixed emitter-collector spacing. A sapphire part has therefore been adopted for this purpose. The spacing required, some 0.006 in., is to be held, even though the collector thimble is expected to lengthen 0.009 in. more than the emitter thimble. Ordinarily, this would cause the spacing to be increased, but the introduction of a diaphragm closure will allow air pressure to hold the anode and cathode in contact with the spacer. Further, the sapphire spacer has its c-axis oriented along the direction of loading, thus minimizing problems with creep. Figure 4 is a cutaway drawing of the assembled unit.

Most of the parts have been prepared. After coating the inside of the emitters with Durak-B, assembly of the diodes will commence.

Phase 2 – Diode Performance Characteristics

The 150-w diode was first operated on December 7, 1961. This diode used a cylindrical emitter, 84 cm^2 in area, and was heated by a combination of radiation from a filament and electron bombardment. The purpose of the first series of tests was to establish the critical operating parameters of the diode and to compare its performance with that of the smaller diodes undergoing test at Atomics International. To this end, optimized operating points and volt-ampere curves were obtained. These data are discussed in detail in the previous report.[1] The maximum electrical output power density was 1.72 w/cm^2, with an overall efficiency of 7.8%, and an optimum output voltage of 0.7 v, at an emitter temperature of 1540°C. At a 1400°C emitter temperature, the power density was 0.9 w/cm^2; the overall efficiency, 4.3%; and the optimum output voltage, 0.45 v. Corresponding data were obtained during the present report period. However, because of the cesium leak which occurred on December 20, the tests made in January were restricted to the 1300 to 1400°C temperature range. This precaution was taken to prolong the life of the heater filament and of the diode itself. The corrected emitter temperatures for the January runs are plotted against total operating time in Figure 5. This record begins at 25.8 hr, the cumulative

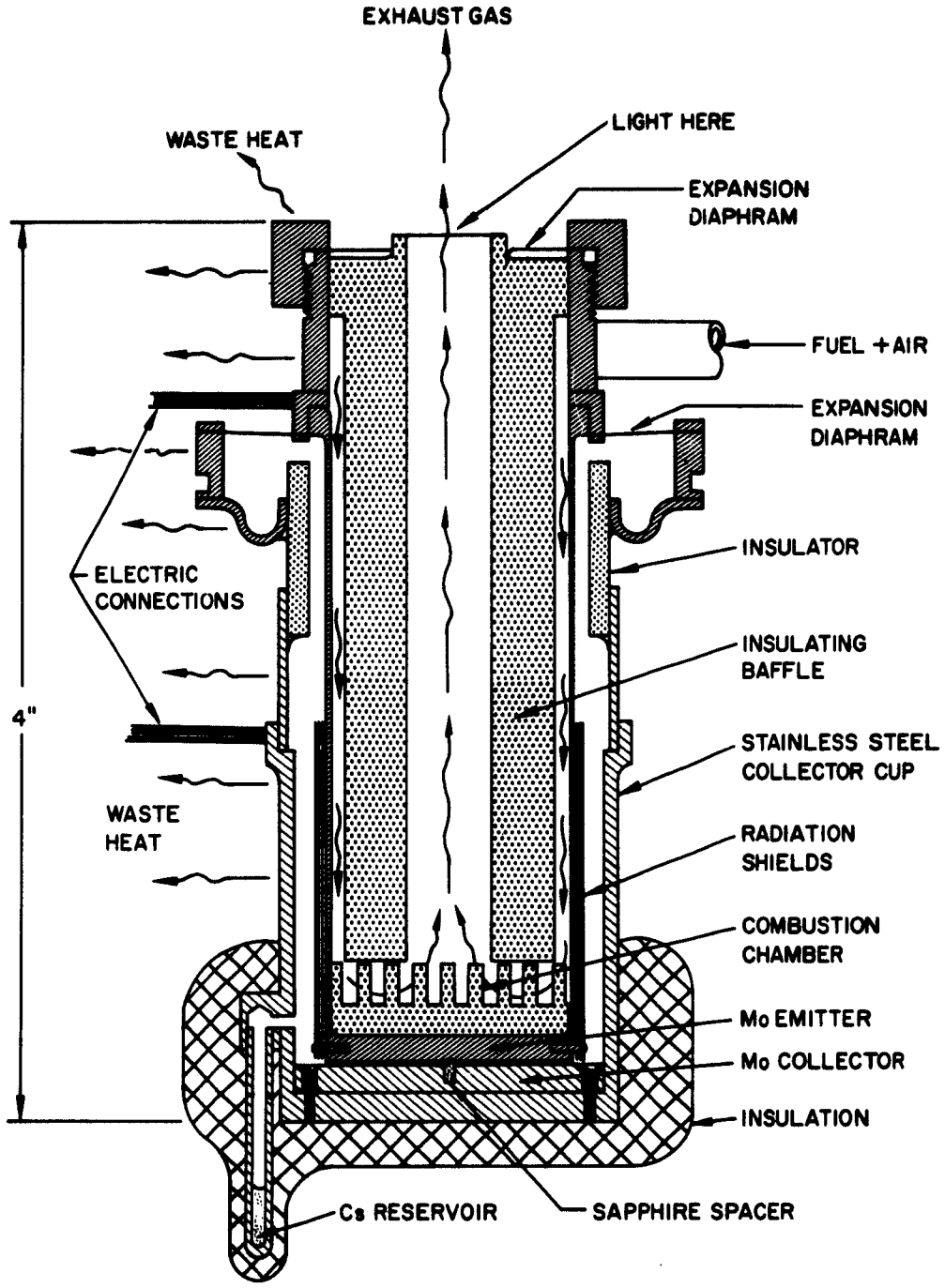

Figure 4. Second Demonstration Flame-Heated Thermionic Diode

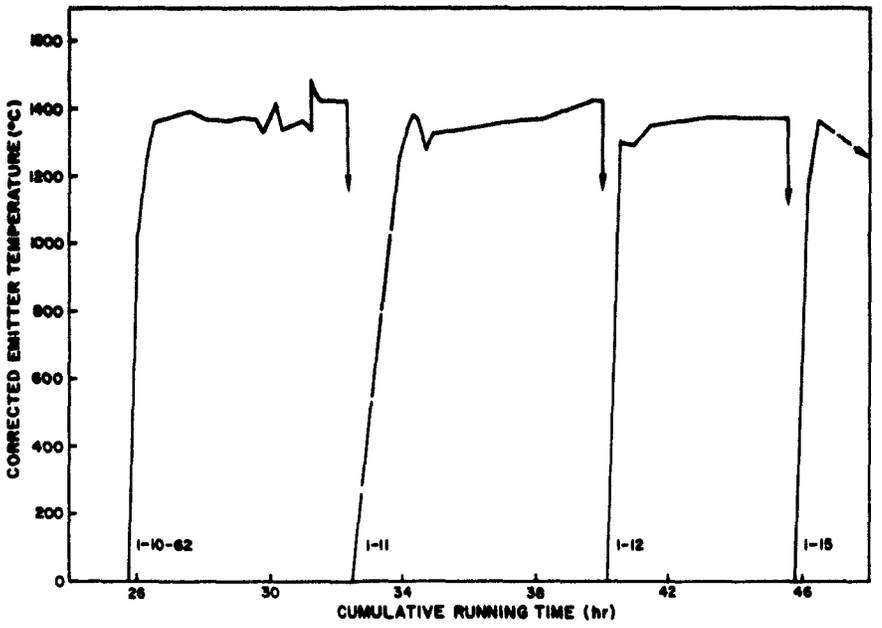

Figure 5. 150 w(e) Diode Operating History

time logged in December, and extends to the data for January 15, at which time the cesium was exhausted. A total running time of 34 hr was accumulated a T_e's above 1300°C; and, of these, 10 hr were above 1400°C.

Triggered Diode

Because of the concern about the loss of cesium, the goal of the January tests was to investigate the ignition characteristics of the 150-w diode, in order to evaluate its possible use as an element of a triggered diode system.[1,3] The proposed system is shown on Figure 6. Two cesium vapor converters are connected to a center-tapped transformer, as shown. If Converters 1 and 2 could be made to fire alternately, alternating current would be generated in the transformer's primary winding. This current could then be transformed to any desired voltage and rectified. In this scheme, one would exploit the ability of a thermionic diode to operate in either the ignited or the unignited mode. The transition between these would be triggered by an electrical pulse. Figure 7 shows a typical volt-ampere curve, characteristic of bi-stable operation. Note that the current and voltage of the diode can follow back and forth, either along the extinguished mode curve or along the ignited mode curve. However, if the ignition point is reached in the unignited mode, the diode then quickly "fires"

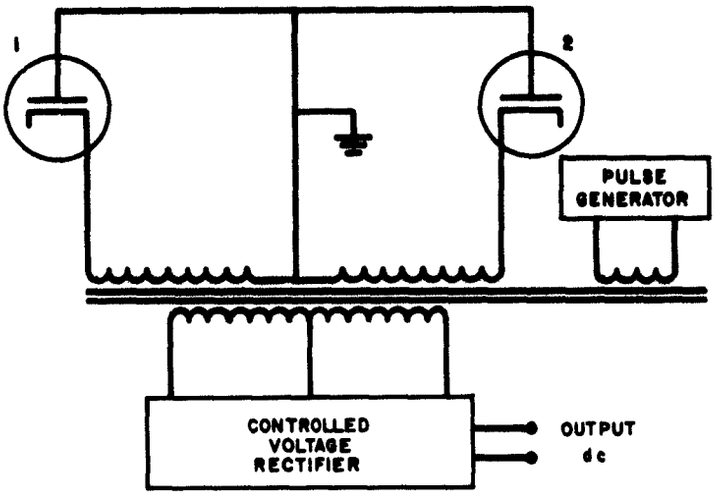

Figure 6. Triggered Diode Power Inversion System

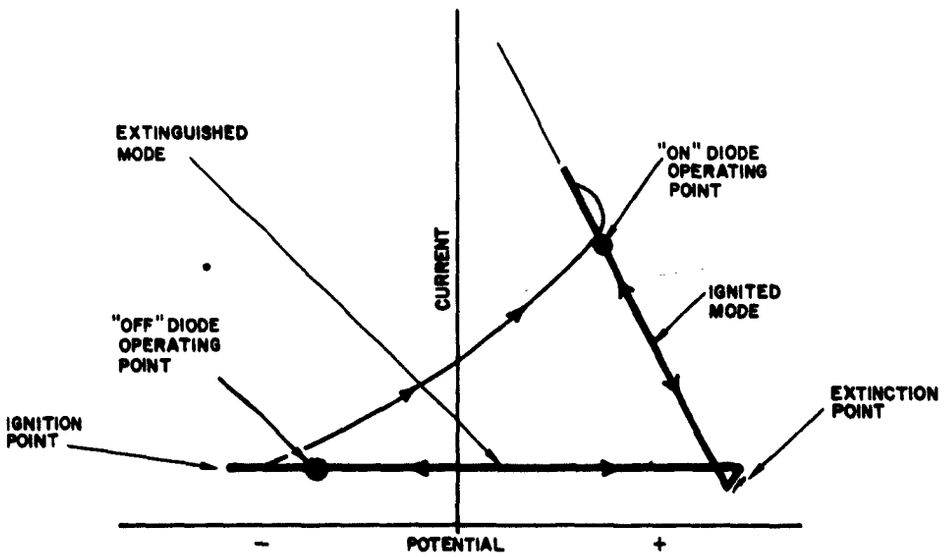

Figure 7. Typical Bi-Stable Diode Volt-Ampere Curve

into the ignited mode. Conversely, if the extenction point of the ignited mode is reached, the diode will then operate in the unignited mode.

The desired operating sequence begins with Diode 1 at the "on" point and Diode 2 at the "off" point. When the pulse generator fires, a potential is induced in the primary of the transformer, and Diode 2 is driven to its ignition point. The sudden firing of Diode 2 drives Diode 1 to the extinction point. Diode 1 then assumes the "off" operating point, and Diode 2 the "on" operating point. The next signal from the pulse generator is in the opposite sense, and the diodes are returned to their original operating points.

In order that this scheme be practical, the diodes must have good efficiencies at the ignited mode operating point, and a low current drain in the "off" position. In addition, the absolute value of the negative emf at the ignition point must be greater than the positive emf of the "on" operating point, so that the diodes will not spontaneously fire one another. The January tests of the 150-w diode were therefore designed to establish the conditions under which this diode could be operated as a triggered diode, and to attempt to determine the net power output obtainable from this type of operation.

The studies were made, using a 60-cycle transformer in series with the diode load. An examination of the volt-ampere figures thus produced shows that, for a given emitter temperature in the 1300 to 1425°C range, a definite sequence of volt-ampere curve shapes are generated as the cesium reservoir temperature is raised from, say, 30°C below the optimum T_{Cs} to temperatures markedly above the optimum T_{Cs}. Figure 8 illustrates this, and shows ten typical volt-ampere curves obtained in this study. The sail-shaped curves marked 34-1, 28-2, 28-5, and 28-1 have suitable characteristics for triggered diode operation. It is of interest to note that the observed T_{Cs} values range from 5°C below optimum to 35°C above optimum for these curves. Curves 28-4, 29-2, and 29-4 have observed T_{Cs} values of 10 to 15°C below the optimum, and show a tendency toward the desired sail-shape, but their ignition emf's are too positive. Under these conditions, each diode would "fire" the other. Curves 28-3, 29-1, and 32-1 are typical of those for which the observed T_{Cs} is 25 to 35°C below the optimum value. These conditions are obviously unsuitable for triggered diode operation. It thus appears that one must operate a triggered diode at or above its optimum T_{Cs}, in order to achieve a bi-stable condition.

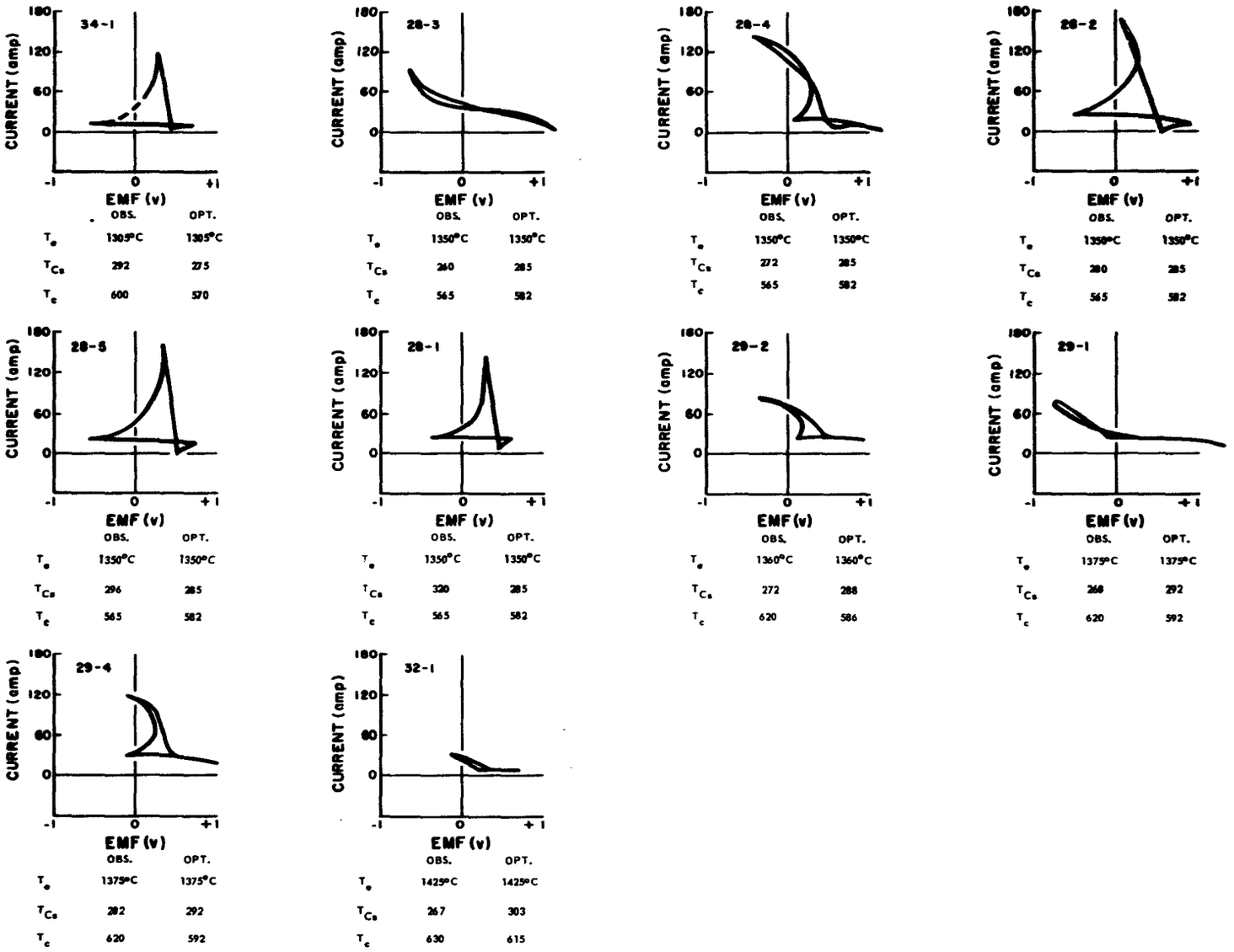

Figure 8. 150 w(e) Diode Volt-Ampere Curves

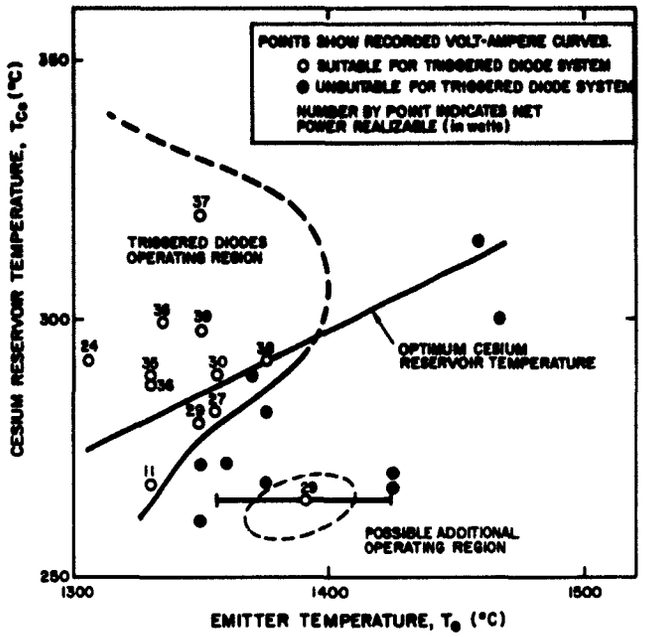

Figure 9. Operating Regions for Triggered Diode Power Inversion System

It is of interest to estimate the net output of a pair of diodes operating in the proposed way. One diode would be delivering power at its maximum rate, the other would dissipate a fraction of it, and the remainder would be available to drive the transformer. Figure 9 shows a number of suitable operating points, plotted as T_{Cs} vs T_e. A curve of optimum T_{Cs} is also given, and the net power adjacent to the points. Also shown are a number of unsuitable operating points. That is, these points did not exhibit a bi-stable type of volt-ampere curve which could be used in a triggered diode power inversion system.

Note that the suitable points so far observed all lie below a T_e of 1400°C. Based upon present data, it appears that, at some temperature between 1400 and 1450°C, sufficient ions are emitted from the surface so that volume ionization is not required for space charge neutralization. At this point, the bi-stable mode of operation disappears.

Also note that suitable operating points lie at cesium reservoir temperatures a little below, and a large amount above, optimum. The scatter in the net power realizable for the suitable operating points is too great to conclude anything at present.

Finally, note that Figure 9 indicates a possible additional operating region, at a lower T_{Cs} and a higher T_e than for the rest of the suitable points. Although only one volt-ampere curve was recorded from this region, some data were taken with the 150 w(e) diode, in which the emitter power was held constant and the cesium reservoir was cooled and heated again slowly. The volt-ampere curve was observed constantly on the oscilloscope, and the coordinates of the ignition point were recorded.

These data (See Figure 10) show that the ignition voltage and current generally follow that observed by Kitrilakis.[4] Both during heating and cooling of the cesium reservoir, the ignition voltage changed rapidly at a T_{Cs} of 280 to 285°C. Kitrilakis observed a discontinuity at this temperature. In the temperature range over which the data were taken, the on-diode operating point is 0.2 to 0.3 v. Therefore, a negative ignition voltage, less than this, could be used in a triggered diode power inversion system. Thus, from the present data, possible areas of operation are shown to exist at $T_{Cs} < 260$ or 250°C, and also at $T_{Cs} > 280$ or 285°C, for the temperature range indicated in Figure 10. This phenomenon bears further investigation.

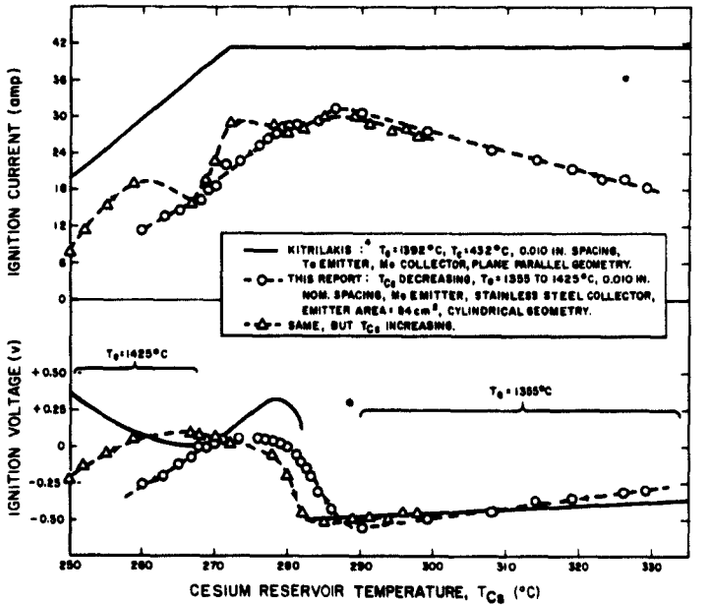

Figure 10. Observations on Ignition Point as a Function of Emitter Temperature

Diode Switching

The inducement of the transition between modes was studied briefly, using a capacitor discharge as the triggering mechanism. It was found that a 12-v charge on a 2000 mfd capacitor would fire the diode when operating at T_e = 1350°C, T_{Cs} = 287°C, and T_c = 560°C. In addition, a 12-v charge on a 4000 mfd capacitor would extinguish the diode, under the same conditions.

TASK B – HEAT SOURCE DEVELOPMENT

Phase 1 – Aspirated Burner Development

No work was done on this phase during this quarter.

Phase 2 – Fan-Powered Burner Development

High Efficiency Heater Development

In the light of the work done under Phase 5, it appears that burner heat exchanger assemblies of inherently high efficiency are definitely required, in order to attain the highest power-to-weight ratios possible in portable thermionic power sources. In pursuit of this goal, a number of experiments were conducted, using the combustion chamber and reversing flow regenerative heat exchangers shown in the conceptual design.[1] A cross section of the furnace used in High-Efficiency Heater Experiment No. 1 is shown on Figure 11. By means of a system of solenoid valves and a cycle timer (not shown), the combustion air was forced alternately, first up and then down, through the stacked screen regenerators and the combustion chamber. Propane was injected into the combustion chamber through a fluid-cooled tube. Mixing and burning took place in the combustion chamber. Heat was transferred to the silicon carbide tube walls lining the combustion chamber, and was conducted through the thick-walled tube to the cooling water coils at both the top and the bottom of the furnace. The fraction of the potential chemical energy of the fuel that was absorbed by the cooling water was taken as the heating efficiency for this experiment.

It was difficult to obtain complete combustion in this experiment. Evidently, there was insufficient time for the fuel to mix with the air and then to burn before the mixture was swept into one of the regenerators and quenched. In an attempt to remedy this situation, a baffle plate, made of foam silicon carbide, was inserted into the combustion chamber during Runs Number 2 and 3. This baffle plate also protected the bottom regenerator from overheating as a

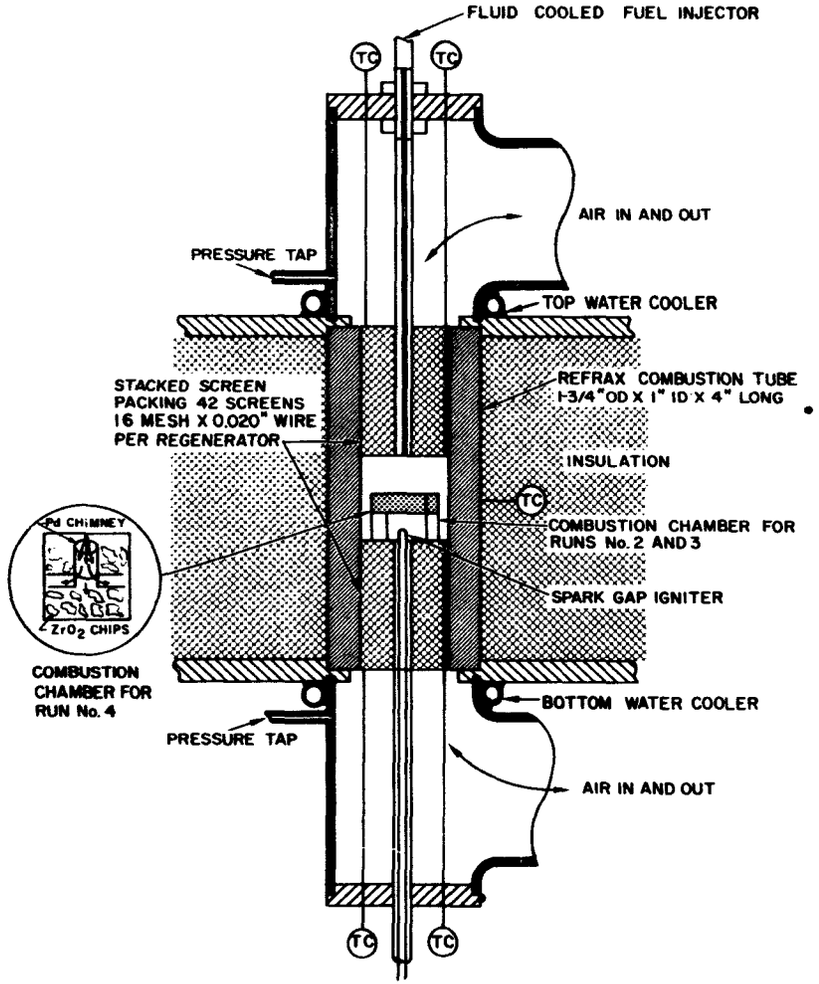

Figure 11. High-Efficiency Heater Experiment No. 1

TABLE I

RESULTS OF HIGH EFFICIENCY BURNER EXPERIMENT NO. 1

	Run Number		
	2	3	4
Potential Heat Input, Q_F (w)	645	965	1470
Air-gas Ratio	1.12	1.48	1.37
Heat to Heat Sink, Q_e (w)	259	364	580
Heating Efficiency, η_H	0.40	0.38	0.39
Heat Flux to Combustion Chamber (w/cm^2)	10.3	14.5	23.2
Combustion Chamber Temperature (°C)	360	470	820
Combustion Chamber Temperature Swing (°C)	20	25	30
Cycle Time (min)	2	2	0.5
Air Supply Pressure (in. H_2O)	1.2	-	9-13.4

result of flame impingement. In Run Number 4, a bed of zirconia chips (-6 +8 mesh) was packed into the combustion chamber. At the center of the bed was a palladium chimney, designed so that the fuel could be injected into the center of the bed, no matter which way the air flow was going.

The results of High Efficiency Burner Experiment No. 1 are given in Table I. Notice that the heating efficiencies (η_H) are high, even considering the rather low combustion chamber temperatures which were attained. The relationship between combustion chamber temperature and heat flux to the combustion chamber indicates that the wall thickness of the silicon carbide combustion tube was twice that required to attain the proper combination of combustion chamber temperature and heat flux.

One of the obvious objections to the use of a reversing-flow heat exchanger in a diode heater is the cyclic temperature variation occasioned by the cyclic air flow reversals. These are shown, in Table I, to be 20 to 30°C. This variation was found to be chiefly a result of greater combustion efficiency for downward air flow than for upward. Greater care in the design, so that downward and upward air flow would have the same combustion efficiency, will greatly reduce the already small temperature variation.

The preparation of High Efficiency Burner Experiment No. 2 was started. This will include a thinner combustion tube, a symmetrical combustion chamber, a larger fluid-cooled fuel injector, and regenerators made of silicon carbide foam drilled with small holes. Construction of this experiment has been deferred until a simpler burner is developed for the demonstration diode, due at the end of GFY 1962. Nevertheless, as will be shown under Phase 5, development of a high-efficiency diode heater is a definite necessity.

Demonstration Diode Heater Development

In view of the many unsolved problems in the development of a heater with high heating efficiency, we felt that the present demonstration diode heater should have a simpler (although less efficient) heater, to ensure having a workable unit by the end of GFY 1962. One concept of how the diode heater and the diode would be integrated is shown in Figure 4. Notice that the diode has a plane-parallel geometry, with the emitter and collector at the bottom of two concentric thimbles. The combustion chamber is at the bottom of the inner thimble. Premixed air and fuel enter at the top of the thimble and flow down through the annulus between

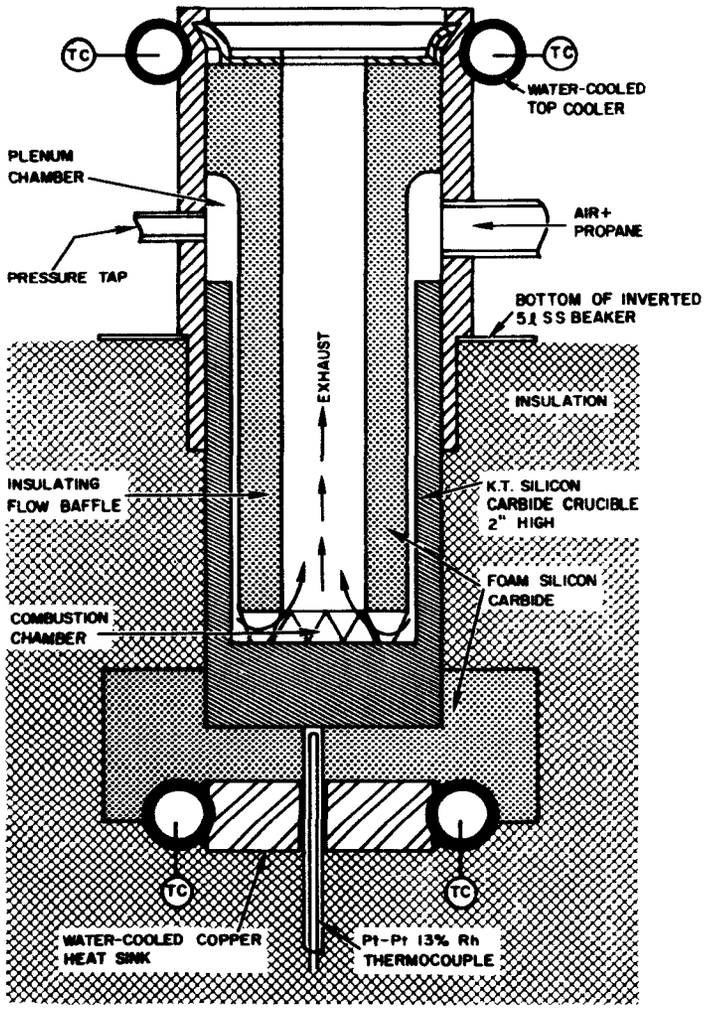

Figure 12. Experimental Setup for Heater Experiment Runs DD-1 to DD-3

TABLE II

RESULTS OF RUNS DD-1 TO DD-3

	Run Number		
	DD-1	DD-2	DD-3
Heat in, Q_F (w)	615	1080	960
Heat out to:			
Heat Sink, Q_e	31	33	not used
Top Cooler, Q_I	not measured		143
Heating Efficiency, η_H	0.05	0.03	0.15
Heat Flux, q_e (w/cm^2)	5	5	22
Combustion Chamber Temperature (°C)	502	602	1350
Air Supply Pressure (in. H_2O)	1.6	2.7	-

the molybdenum thimble and the insulating baffle. In this way, the joint at the top of the molybdenum thimble is kept as cold as possible. The fuel and air burn in a combustion chamber which is made by sawing two rows of grooves, at right angles to each other, in the top of a KT silicon carbide disc. The resultant posts hold the flame and conduct the heat directly to the molybdenum emitter. The exhaust gas passes out through the center hole. The insulating baffle between the exhaust gas and the fuel-air mixture is designed so that the mixture is heated up to its ignition point, but not beyond. In this way, flashback is not experienced.

Twenty-seven runs were made on a number of variations of the idea shown in Figure 4. Experimental setups for each variation will be briefly described, and the data for each variation will be presented. Graphs will be presented, comparing the different performance parameters for all runs, and the direction for future development of this type of burner will be indicated.

Runs DD-1 to DD-3

Figure 12 shows the experimental setup which was first devised to test diode heater designs for the demonstration diode. This first experiment was designed so that the air and propane fuel could be brought to the top plenum chamber separately, so that mixing would take place as the gases passed down the annulus to the combustion chamber. However, we found that better operation was obtained if the air and propane were mixed before flowing into the plenum chamber. The combustion chamber is as shown in Figure 12 for Runs DD-1 and DD-2. The bottom of the insulating flow baffle was serrated, to provide more surface for combustion. The diameter of the exhaust tube was made as large as practical, to reduce the pressure drop. In Run DD-3, the insulating flow baffle was raised, to allow a single row of silicon carbide chips (-3-1/2 +4 mesh) to line the bottom of the silicon carbide crucible. The results of this series of runs are given in Table II. In Runs DD-1 and DD-2, the heat absorbed by the copper heat-sink was measured by determining the temperature rise and flow-rate of the cooling water. Cooling water flowed through the top cooler, but its flowrate and temperature rise were not measured. In Run DD-3, the water to the copper heat sink was shut off, and the heat absorbed by the top cooler was used to compute the heating efficiency and heat flux. All heat fluxes were based upon an emitter area of 6.4 cm^2. In Runs DD-1 and DD-2, a Pt - Pt 13% Rh thermocouple was used to determine emitter temperature. In Run DD-3, the thermocouple failed and the reported temperature was measured by a pyrometer, observing the crucible through the exhaust duct.

TABLE III

RESULTS OF RUNS DD-4 TO DD-8

	Run Number			
	DD-4	DD-6	DD-7	DD-8
Heat in, Q_F (w)	205	563	920	410
Heat out to:				
Top Cooler, Q_I	21	12	12	86
Heating Efficiency, η_H	0.10	0.02	0.01	0.21
Heat Flux, q_e (w/cm^2)	3	2	2	14
Combustion Chamber Temperature (°C)	933	816	1131	1098
Air Supply Pressure (in. H_2O)	-	4.5	9.0	3.5

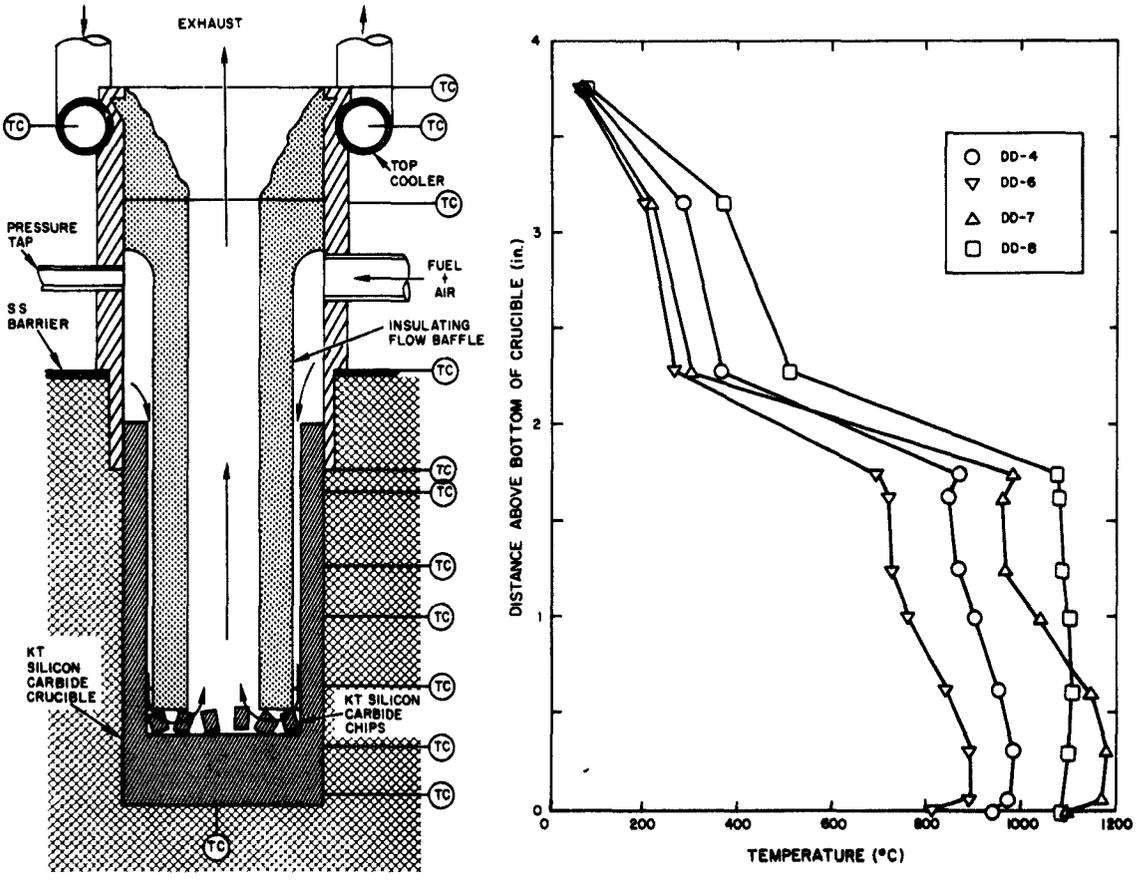

Figure 13. Experimental Setup and Temperature Distribution for Heater Experiment Runs DD-4 to DD-8

Runs DD-4 to DD-8

In this series of measurements, the experimental setup shown in Figure 12 was repaired and modified, in order to give more information. The heat sink was removed, the KT silicon carbide crucible was lowered somewhat, and more thermocouples were added, as shown in Figure 13. The heat absorbed by the top cooler was then taken as a measure of the heat flux into the simulated emitter. Due to the success of Run DD-3, a layer of KT silicon carbide chips over the bottom of the crucible was used as the combustion chamber. The results for Runs DD-4 to DD-8 are shown in Table III. Note that, except for Run DD-8, the heating efficiencies and the heat fluxes are very low. However, Run DD-8 appears to have significantly better performance on all counts. Some understanding of why Run DD-8 was better can be had by examining the temperature traverses in Figure 13. In Runs DD-4, 6, and 7, there is a temperature gradient along the silicon carbide crucible, showing that the bulk of the heat is released at the bottom of the crucible and is conducted upward. In Run DD-8, the temperature of the entire crucible is essentially constant. This indicates that combustion took place at the top of the crucible. Thus, heat is not being transferred at the intended location, and the results do not indicate proper performance.

Runs DD-9 to DD-12

The remainder of the demonstration diode heater experiments described in this report used the same experimental setup, with only minor changes in the shape of the insulating flow baffle and the details of the combustion chamber. The second demonstration diode heater test setup is shown in Figure 14. In this setup, the insulation is completely sealed off, so that none of the propane-air mixture can leak through the insulation. Also, a heat sink was re-installed at the bottom of the heater, next to the combustion chamber. A photograph of this apparatus, together with some of the internal parts, is shown in Figure 15. During operation, the entire surface of the stainless steel beaker can be touched with the hand, which shows that almost all of the heat transferred from the flame is collected in one of the water coolers. The pieces shown on the card at the bottom of Figure 15 are, from left to right, the insulating flow baffle, expansion diaphragm, the side of the silicon carbide crucible, and the bottom of the crucible. These four pieces are assembled as shown in Figure 16. The insulating flow baffle was constructed out of foam silicon carbide,

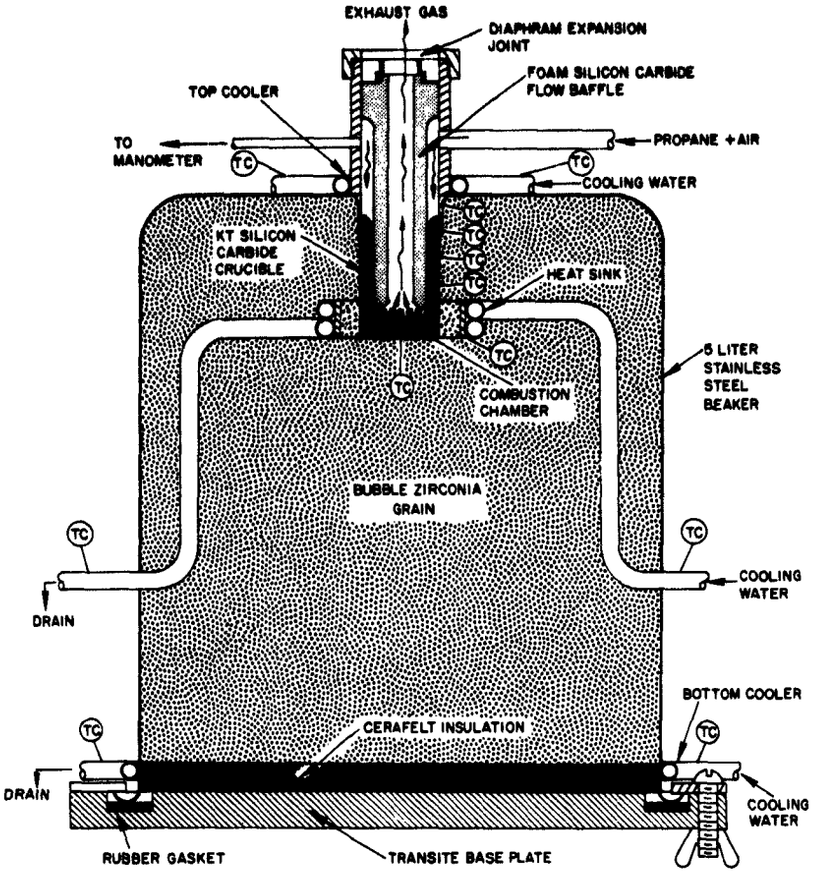

Figure 14.
Test of Second Demonstration Diode Heater

Figure 15.
Test Furnace for Second Demonstration Diode Heater

Figure 16. Insulating Flow Baffle and Combustion Crucible

2414-1846

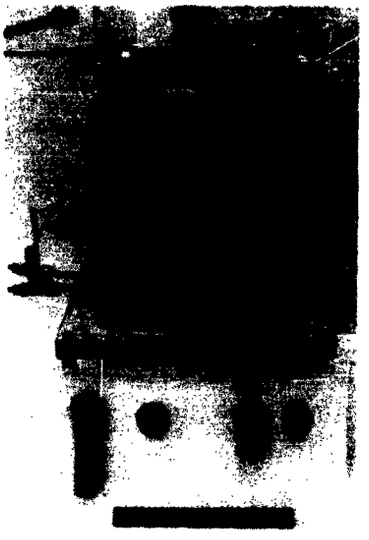

2414-1822

because this material is machinable and has good thermal shock resistance. However, the material is quite permeable to gas; and the outside of the flow baffle was sealed, either with Astroceram cement or a wash of powdered quartz. The diaphragm expansion joint, shown at the right of Figure 16, was found to be a successful way of preventing leakage of the propane air mixture while maintaining flexibility to allow for differential thermal expansion.

The internal arrangements for Runs DD-9 to DD-12 are shown in Figure 17. The thermocouples attached to the outside of the silicon carbide crucible and the stainless steel tube indicated a better temperature profile than had previously been possible. The thermocouples attached to the silicon carbide are Pt - Pt 13% Rh thermocouples, wired on by a piece of platinum wire wrapped around the crucible. The thermocouples on the steel are spot welded Chromel-Alumel. During Runs DD-9, 10, and 11, all thermocouples were working properly. Note that T-1 indicated a temperature considerably higher than T-2, and that temperatures T-2, T-3, and T-4 form a reasonably straight line. However, in Run DD-11, T-3 and T-4 extrapolate to T-1 in temperature. Between Runs DD-11 and DD-12, the thermocouples T-1 and T-2 acted strangely, and T-2 open-circuited. In Run DD-12, an optical pyrometer was used to observe the temperature at the top of the hottest silicon carbide post, as well as at the bottom of the crucible. The bottom of the silicon carbide crucible was thereafter taken as the combustion chamber temperature. It is interesting to note that here, again, the extrapolation of T-3 and T-4 points to temperature P-1. Observed temperature P-1 is subject to positive error, due to shine from hotter surfaces, and negative error, due to emissivity correction. Since the emissivity of silicon carbide is close to one, P-1 is probably higher than the true temperature. In future experiments, a black-body hole will be drilled in the bottom of the crucible to determine what this error might be. However, until a more definite measurement of error is obtained, the observed temperature (P-1) is quoted as the combustion chamber temperature. The results of Runs DD-9 to DD-12 are shown in Table IV. These runs show an acceptable heating efficiency, emitter temperature, and heat flux. However, the air supply pressure is high.

Runs DD-13 to DD-16

In order to reduce the high air supply pressure required in the previous runs, the insulating flow baffle was modified to increase the flow area substantially (See Figure 17). In all other respects, the experimental setup was

TABLE IV

RESULTS OF RUNS DD-9 TO DD-12

	Run Number			
	DD-9	DD-10	DD-11	DD-12
Heat in, Q_F (w)	452	564	923	1230
Heat out to:				
Heat Sink, Q_e	89	119	149	198
Top Cooler, Q_I	45	44	48	48
Bottom Cooler, Q_I	11	4	4	4
Stack Gas, Q_S (by difference)	307	397	722	980
Heating Efficiency, η_H	0.20	0.21	0.16	0.16
Heat Flux, q_e (w/cm^2)	14	19	23	31
Combustion Chamber Temperature (°C)	903	1041	1229	1325
Air Supply Pressure (in. H_2O)	2.3	2.7	6.5	11.9

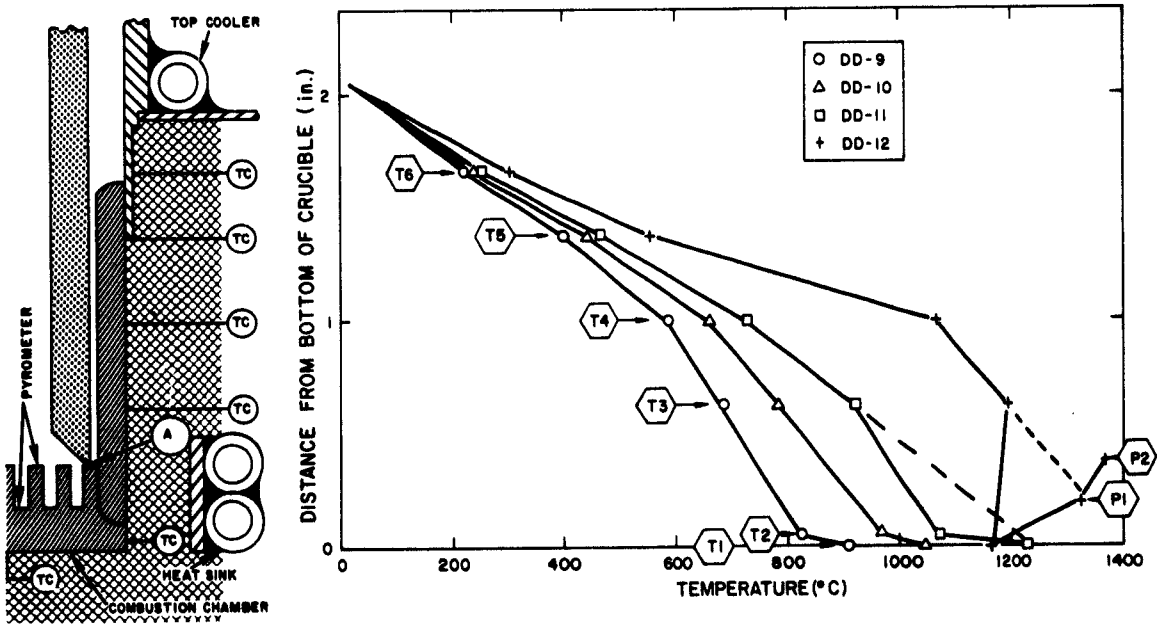

Figure 17. Experimental Setup and Temperature Distribution for Heater Experiment Runs DD-9 to DD-12

TABLE V

RESULTS OF RUNS DD-13 TO DD-16

	Run Number			
	DD-13	DD-14	DD-15	DD-16
Heat in, Q_F (w)	718	1190	1400	1620
Heat out to:				
Heat Sink, Q_e	89	136	143	155
Top Cooler, Q_I	32	99	76	72
Bottom Cooler, Q_I	1	4	4	4
Stack Gas, Q_S (by difference)	596	951	1177	1389
Heating Efficiency, η_H	0.12	0.11	0.10	0.10
Heat Flux, q_e (w/cm^2)	14	21	22	24
Combustion Chamber Temperature (°C)	992	1335	1375	1400
Air Supply Pressure (in. H_2O)	1.6	4.2	5.1	5.3

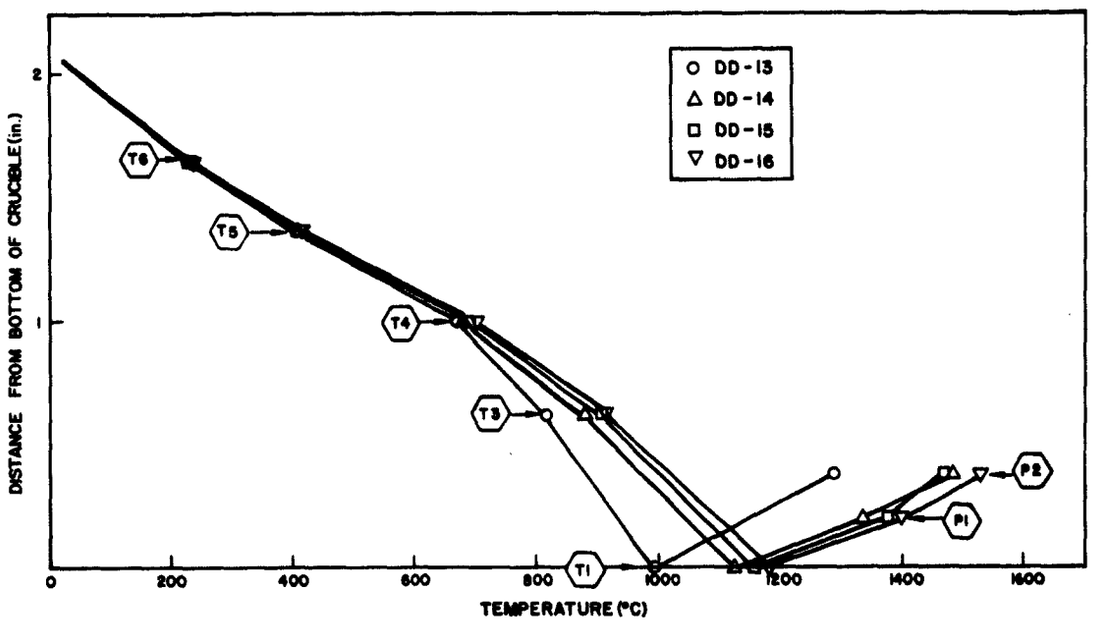

Figure 18. Temperature Distribution for Heater Experiment Runs DD-13 to DD-16

TABLE VI

RESULTS OF RUNS DD-17 TO DD-20

	Run Number			
	DD-17	DD-18	DD-19	DD-20
Heat in, Q_F (w)	1045	1480	1710	472
Heat out to:				
Heat Sink, Q_e	171	172	116	108
Top Cooler, Q_I	64	62	46	42
Bottom Cooler, Q_I	1	3	2	1
Stack Gas, Q_S (by difference)	809	1243	1546	321
Heating Efficiency, η_H	0.16	0.12	0.07	0.23
Heat Flux, q_e (w/cm^2)	27	27	18	17
Combustion Chamber Temperature (°C)	1360	1400	1175	1150
Air Supply Pressure (in. H_2O)	6.1	9.6	9.6	1.8

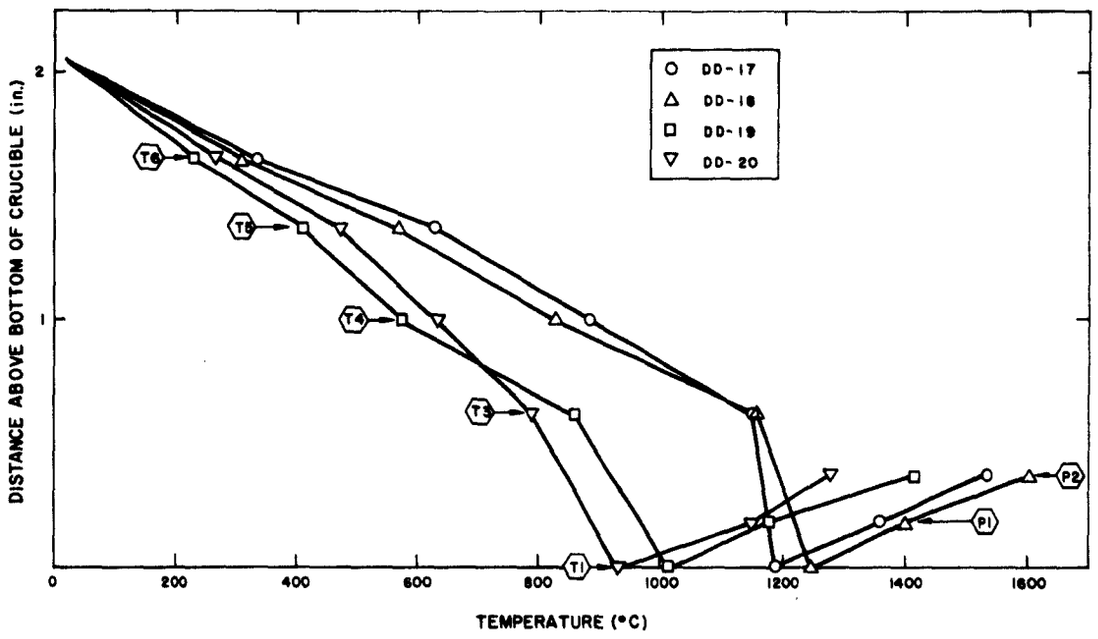

Figure 19. Temperature Distribution for Heater Experiment Runs DD-17 to DD-20

the same. The temperature profiles for these runs are shown in Figure 18. They show good reproducibility. The results shown in Table V indicate that the pressure drop was indeed reduced; however, the heating efficiency was also reduced. The reduced heating efficiency was thought to be due to leakage of the air-fuel mixture through the flow baffle.

Runs DD-17 to DD-20

The same flow baffle was reworked, by sealing with hydrolyzed ethyl silicate in addition to the powdered quartz wash. Also, two 1/8-in. right circular cylinders of KT silicon carbide were placed on top of the combustion chamber to serve as flame holders during the warmup time. The temperature profile, shown in Figure 19, gives more indication that thermocouple T-1 reads low, and that pyrometer measurement P-1 is approximately correct. For some reason, these temperature profiles appear to have quite a different character than the previous ones. The results of this series, tablulated in Table VI, are good, although the pressure drop is somewhat high. Note that Run DD-19 has the highest heat input for the series, but does not have the highest combustion chamber temperature.

Runs DD-21 to DD-27

A new insert was turned out of silicon carbide and sealed with quartz powder and hydrolyzed ethyl silicate. The insert was shaped as shown in Figure 14, and no pebbles were used as flame holders. The temperature profiles for this series, shown in Figure 20, show a high degree of reproducibility during the series. Here again, temperatures T-3 and T-4 extrapolate to P-1. The unusual shape of the profile for Run DD-22 indicates that some pre-ignition occurred. Also, Run DD-26 was out of pattern, having a lower-than-normal P-1 temperature. Although all the other experiments were quiet, Run DD-26 exhibited a definite whistle. The results of this series (tabulated in Table VII) indicate that Run DD-26 had the highest heat input; and is another case like Run DD-19, where the flame was almost blown out of the flame holder. This series of runs shows the best performance, with low air supply pressures and high emitter temperatures, heat fluxes, and heating efficiencies. However, the foam silicon carbide is not entirely satisfactory as a flow baffle. Runs DD-27 and DD-23 were intended to be duplicate runs. They had the same heat input and the same air supply pressure requirement. However, the heating efficiency,

TABLE VII

RESULTS OF RUNS DD-21 TO DD-27

	Run Number						
	DD-21	DD-22	DD-23	DD-24	DD-25	DD-26	DD-27
Heat in, Q_F (w)	492	810	1085	1310	1515	1700	1065
Heat out to:							
Heat Sink, Q_e	127	178	180	176	184	151	151
Top Cooler, Q_I	54	72	185	204	182	154	173
Bottom Cooler, Q_I	1	2	3	2	5	3	2
Stack Gas, Q_S (by difference)	310	558	717	928	1144	1392	739
Heating Efficiency, ηH	0.26	0.24	0.18	0.13	0.12	0.09	0.14
Heat Flux, q_e (w/cm^2)	17	20	28	28	28	29	24
Combustion Chamber Temperature (°C)	1080	1260	1400	1425	1450	1285	1300
Air Supply Pressure (in. H_2O)	0.5	1.3	2.0	2.7	3.3	4.1	2.1

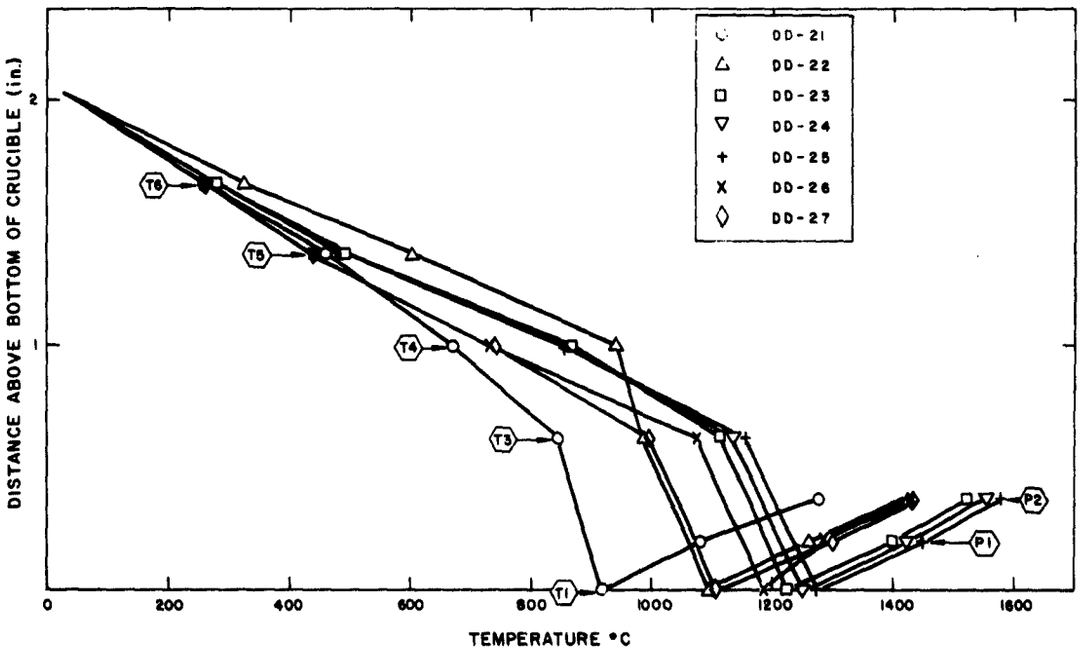

Figure 20. Temperature Distribution for Heater Experiment Runs DD-21 to DD-27

heat flux, and emitter temperature were considerably lower in Run DD-27. On disassembly, we discovered that this deterioration was due to severe cracking in the silicon carbide flow baffle, which allowed appreciable short circuiting of the fuel-air mixture.

Comparison of All Runs

Figures 21, 22, 23, and 24 compare all demonstration diode heater data in different ways. They show a general unity between series. That is, general trends are evident in several different series.

Figure 21 exhibits the relationship between the combustion chamber temperature and the heat input. Note that, in general, increased heat input leads to increased combustion chamber temperature. However, it is definitely shown that there is a point at which this combustion chamber will no longer hold the flame, and the temperature drops as the heat input rises. The series of runs shown in Table VII appear best in the thermionic temperature region (1300 to 1500°C)

Figure 22 shows the relationship between heating efficiency and the combustion chamber temperature. Note that the efficiency usually drops with increased temperature. The drop is most rapid as the maximum temperature for the experiment is reached. Note that, if above-optimum heat inputs are employed, the heating efficiency can increase with combustion chamber temperature, and higher combustion chamber temperatures can be obtained by curtailing heat input.

Figure 23 shows the relationship of heat flux to combustion chamber temperature. It would seem reasonable that this relationship would be set by the heat sink configuration. Data tabulated in Tables IV, V, VI, and VII are taken with the exact same heat sink. The heat sink was never disassembled during this period. However, it is clear (from Figure 23) that each of these series of runs falls on a separate line; and these lines differ substantially from each other. This result might mean that the combustion is taking place at different areas in the combustion chamber; areas which have considerably different thermal resistances to the heat sink.

Figure 24 indicates the relationship between the air supply pressure and the combustion chamber temperature. Note that, for a given run, the supply pressure increases exponentially with combustion chamber temperature. Note

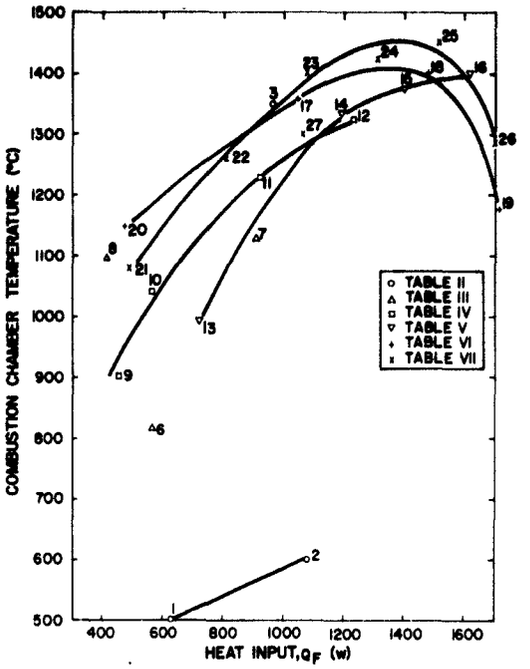

Figure 21. Combustion Chamber Temperature vs Heat Input (Runs DD-1 to DD-27)

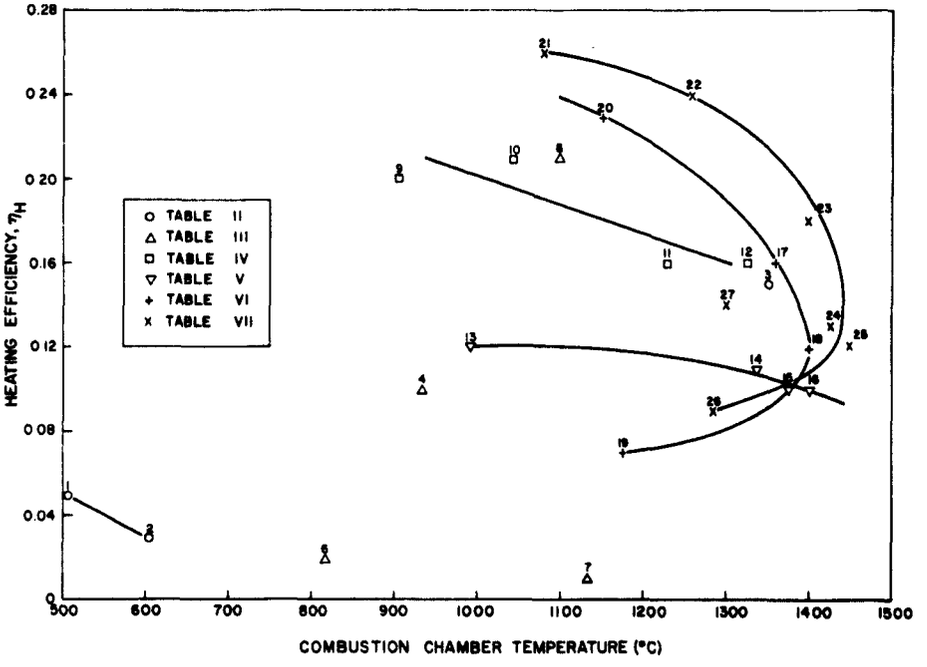

Figure 22. Heating Efficiency vs Combustion Chamber Temperature (Runs DD-1 to DD-27)

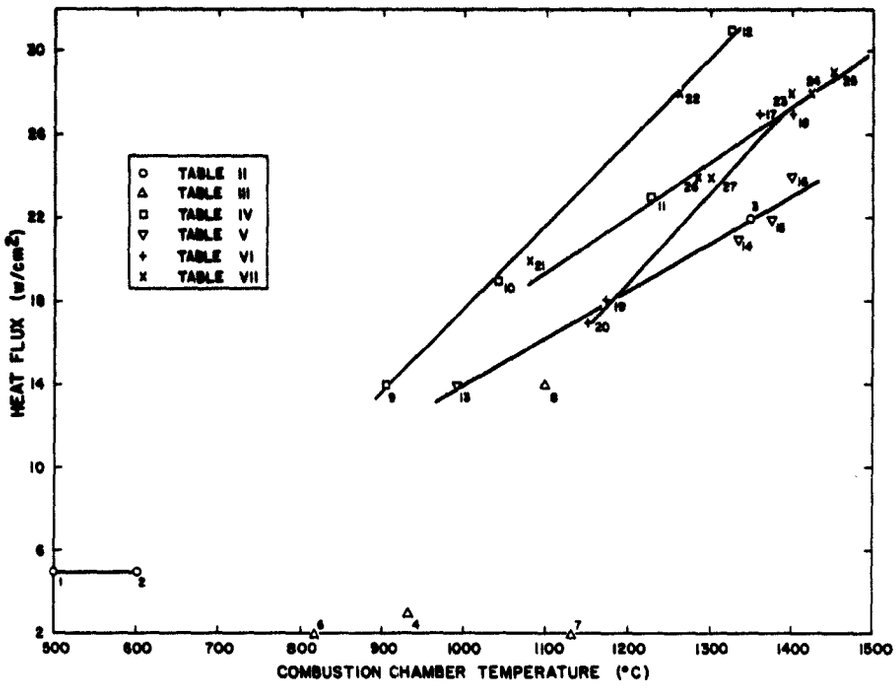

Figure 23. Heat Flux vs Combustion Chamber Temperature (Runs DD-1 to DD-27)

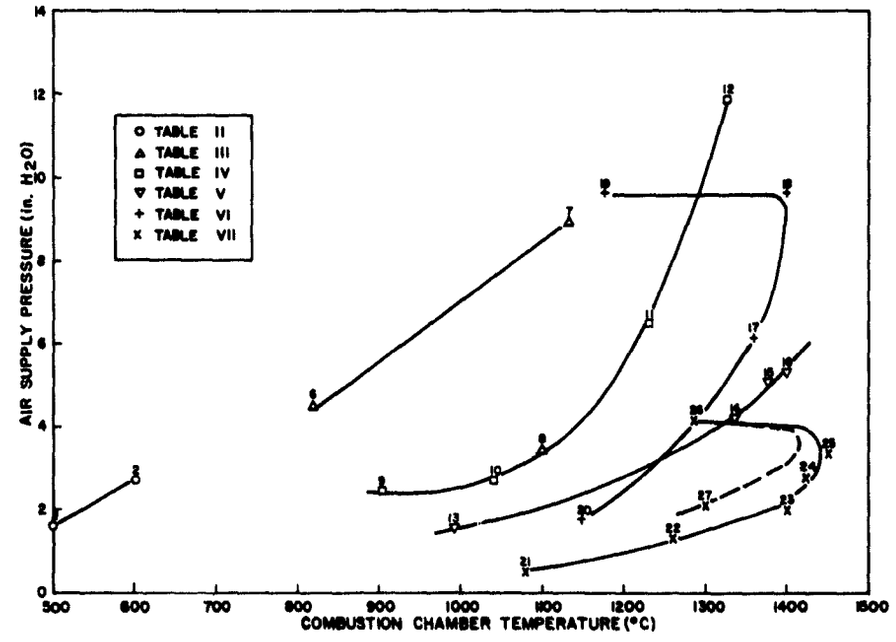

Figure 24. Air Supply Pressure vs Combustion Chamber Temperature (Runs DD-1 to DD-27)

that, in two cases, the optimum fuel input was exceeded. The fact that the air supply pressure did not increase, while the combustion chamber temperature dropped, indicates that the flame was almost completely blown out of the combustion chamber. The series of runs shown in Table VII is again the best, since it has the highest temperature at the lowest air supply pressure.

Phase 3 – Temperature Control

A capsule, containing a fluid at its critical point, is being considered as a tamper-proof temperature controller for the cesium reservoir. To this end, some more calculations have been made. As shown in Figure 12 of Reference 1, the Rayleigh number, which is known to govern the natural convection heat transfer capabilities of a liquid, goes through a very sharp maximum at the critical temperature. It seems, at first thought, that, in order to attain this unique critical point, one must fill the tube with exactly the right amount of fluid, so that the critical temperature and critical pressure are attained at the same time. If too much liquid were introduced into the tube, the liquid might expand until it filled the entire tube and then, on expanding further, generate a very high pressure. Also, if too little liquid were added to the tube, the liquid would completely evaporate before the critical temperature was reached, and the full effect of heat transfer at the critical point would not be realized.

Figure 25 shows the pressure-temperature relationship for a tube filled with sufficient water, so that the weight of the water divided by the volume of the tube equals the critical density for water. It also shows the relationship for 10% and 20% over the critical density, as well as 10% under the critical density. Note that, up to within one degree Fahrenheit of the critical temperature, no difference is possible among the different fillings. For fillings greater than the critical density, the pressure increases at a greater rate, after the tube is entirely filled with liquid. However, the effect is quite small, for reasonable variations from the critical density. This figure was computed from the readily available data on the thermodynamic properties of steam.[5] Data in the neighborhood of the critical point are somewhat sketchy. Therefore, the expanded scale drawing of what happens at the critical point is only qualitatively correct.

One experiment was attempted on critical temperature control during this quarter. The water-filled tube used in the experiments reported previously was reassembled, with the 1/4-in. copper bar supplying heat only to the end of the

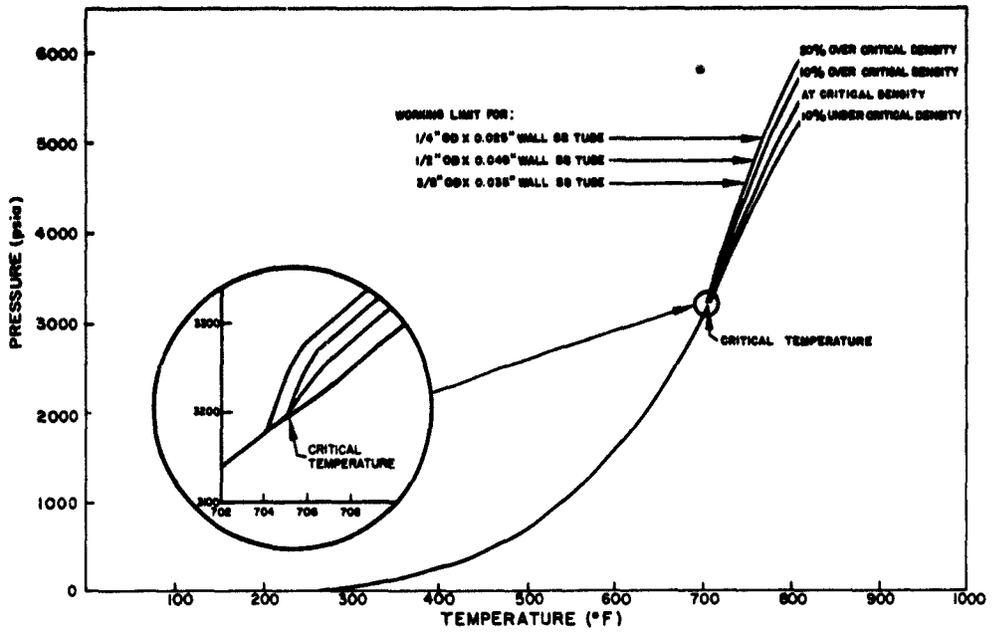

Figure 25. Pressure-Temperature Relationships for Water-Filled Constant Temperature Tubes

tube, instead of to the bottom inch of the tube, as had previously been the case. No temperature control region was observed in this experiment, and indications were that natural convection was unstable. Evidentally, the large heat transfer surface and the higher temperature at one side of the bottom of the tube, in the previous experiment, tended to stabilize natural convection along the tube.

Another tube has been filled with Freon-112 and low-pressure argon gas. The top and bottom portions of the Freon-filled tube have been attached to copper bars, using the previously successful lap joint. Thermocouples will now be attached, and a one-dimensional heat transfer experiment will be attempted. That is, a guard heater will be placed around the experiment, so that all heat entering the bottom copper bar will pass through the filled tube and the top copper bar to the heat sink.

Phase 4 — System Construction and Operation

Diode construction was performed and reported under Task A. The diode heater material is on hand, and the heater will be fabricated as soon as the heater design is completely frozen. Present plans are to construct four flame-heated diodes. We also plan to construct a portable test stand. Low-pressure compressed air and propane must be furnished to the stand, and the electric

TABLE VIII

SELECTED FUEL PROPERTIES[1]

Fuel	Exp. Flame Temp. with Air (°C)	Ignition Temp. with Air (°C)	Fuel Deposition Temp. (°C)	Moles Air Req'd. (10% Excess) Per Mole Fuel
Methane	1870	632	390*	10.5
Propane	1925	481	390*	26
Gasoline				
Regular	1950	280	171	65
100 Octane	1950	429	-	65

*Based upon no cracking below this temperature.

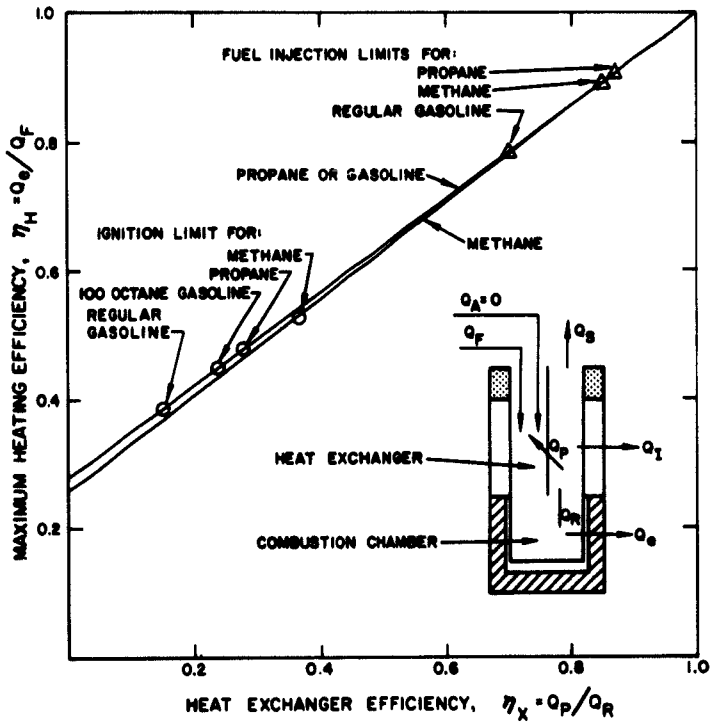

2414-1844

Figure 26. Maximum Heating Efficiency for Various Fuels (T_e = 1500°C, 10% Excess Air, Perfect Flame-Emitter Heat Transfer)

power output will be indicated by an electric light and meters to show voltage and current output. One or more workable diodes will be supplied with the test stand, as a sample product.

Phase 5 – System Design and Analysis

During the last report period, an analysis of the limits and the possibilities of different methods of diode heating was made. The limits are dictated by thermodynamic analysis, and the possibilities are dictated by heat transfer across the heat exchanger and through the insulation.

Thermodynamic Relationships

When a fuel is burned with air, both of which are initially at ambient temperature, the flame has a well-defined maximum temperature. Table VIII gives the experimentally determined temperatures for the stoichiometric combustion of methane, propane, and gasoline; and shows that the adiabatic flame temperatures are all about 1900°C, for these common fuels. In the limiting case of perfect heat transfer from the flame to the emitter, the maximum heat available is that obtained in cooling the gases from the flame temperature to the emitter temperature. In practice, however, only a rather low heat transfer coefficient can be realized for transferring heat from the flame to the emitter. Consequently, a large temperature difference must be maintanied, in order to develop the required heat flux. This effect makes the heating efficiency, η_H, materially less than the theoretical maximum shown in Figure 26. The heating efficiency, η_H, is defined as the ratio of the heat transferred to the emitter, Q_e, to the potential chemical energy of the fuel, Q_F; and is given (for this ideal, limiting case) along the ordinate of Figure 26. Note that, for an emitter temperature of 1500°C, the maximum η_H varies over the narrow range of 0.25 to 0.28, depending upon the fuel used.

As shown in Figure 26, η_H can be increased by introducing a heat exchanger between the exhaust gases and the incoming combustion air and fuel. This has the effect of increasing the flame temperature and the heat available to the emitter. Theoretically, η_H can approach unity as the heat exchanger efficiency, η_X, approaches unity (the heat exchanger efficiency is defined as the ratio of the heat absorbed by the incoming air and fuel, Q_P, to the heat available in the gases leaving the combustion zone, Q_R). A heat exchanger is thus seen to be an essential component of an efficient flame-heated thermionic diode system.

Heat Exchanger Operation, Premixed Air and Fuel

It is of interest to examine ways of operating the heat exchanger. The first of these involves the premixing of the fuel and air, and the subsequent heating of this mixture by the Q_p heat. Under these conditions, the mixture can be heated only to the ignition temperature (Table VIII), in order to avoid premature combustion in the heat exchanger. If premature combustion is allowed to occur, the direction of the heat flow in part of the heat exchanger reverses, and an increasing fraction of the combustion heat is lost to the exhaust gases. Once started, combustion in the heat exchanger tends to be self-perpetuating, and can lead to dangerously high temperatures in the exchanger. Of the common gaseous fuels, methane has the highest ignition point, 632°C. When this air-fuel mixture is preheated to 632°C, and the emitter temperature is 1500°C, methane can yield a maximum heating efficiency of 53%. The maximum heating efficiency of premixed regular gasoline and air is 38%.

The ignition temperatures given in Table VIII are the temperatures at which a mixture of fuel and air burns, if held at that temperature for some time. If preheating is done rapidly, preheat temperatures that are higher than the ignition temperature might be successfully employed.

The maximum heating efficiencies, mentioned previously, are based upon a fixed emitter temperature of 1500°C. However, if the emitter temperature can be lowered, the heating efficiency increases. Figure 27 shows the maximum heating efficiency for gasoline fuels, as a function of heat exchanger efficiency and emitter temperature. The two curved lines represent a conservative estimate of the pre-ignition temperature limitations for regular and 100-octane gasoline, and show the maximum heat exchanger efficiencies known to be possible for premixed fuel at each of the emitter temperatures shown. Note that, as the emitter temperature (T_e) decreases, the η_H increases, and that the known safe value of η_X for premixed air and fuel also increases slightly.

Heat Exchanger Operation, Fuel Injection

It is clear, from the preceding discussion, that the overall efficiency for flame-heated power sources, using premixed fuel and air, is limited. To obtain the ultimate η_O, fuel and air must be preheated separately. The fuel can only be preheated to the temperature at which it begins to form a deposit in the fuel line. This maximum temperature depends upon the fuel composition (with

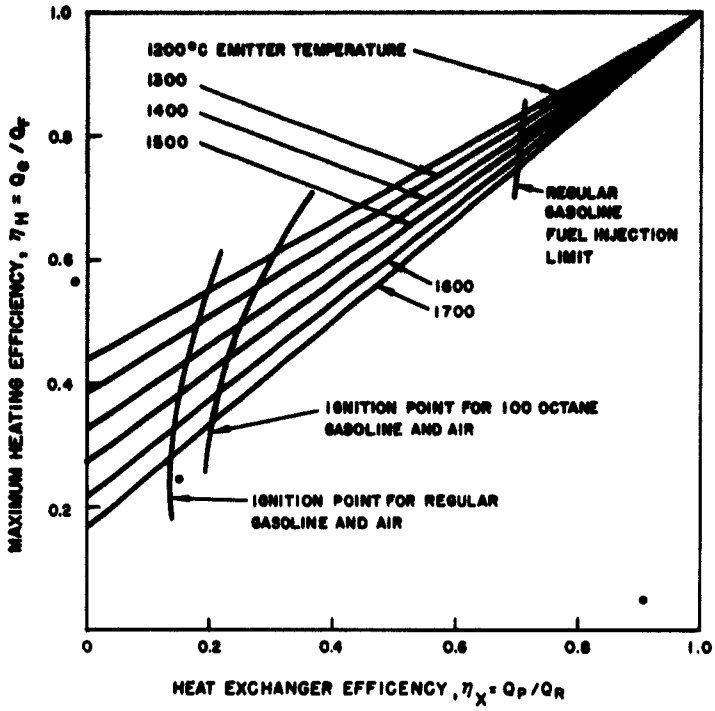

2414-1855

Figure 27. Maximum Heating Efficiency for Gasoline.

particular attention to trace amounts of gums and additives), the wall temperature of the fuel tube, the allowable time between replacements of the fuel tube, and the possibility of burning the deposits out by running air or hot exhaust gas through the fuel tube. The fuel temperature at which deposits begin to occur is known, with certainty, only for regular gasoline (See Table VIII). In any case, the fuel cannot be heated as hot as one would like to heat the air. The two streams must therefore be separated, during passage through the heat exchanger; and, in general, it will be necessary to lead the fuel into the combustion zone through a cooled fuel injector. However, the fuel then has only a short time to mix and burn, making complete combustion more difficult.

The ultimate heat exchanger efficiency is attained if the 10% excess combustion air is preheated to emitter temperature by the exhaust gases which are initially at emitter temperature, and if the fuel is preheated to the deposition temperature (See Table VIII). Using this definition, the maximum η_X, for a T_e of 1500°C, is given in Table IX and is plotted in Figure 26.

It is interesting to note that the maximum η_X for fuel injection is only mildly affected by T_e when regular gasoline fuel is used (See Figure 27). How

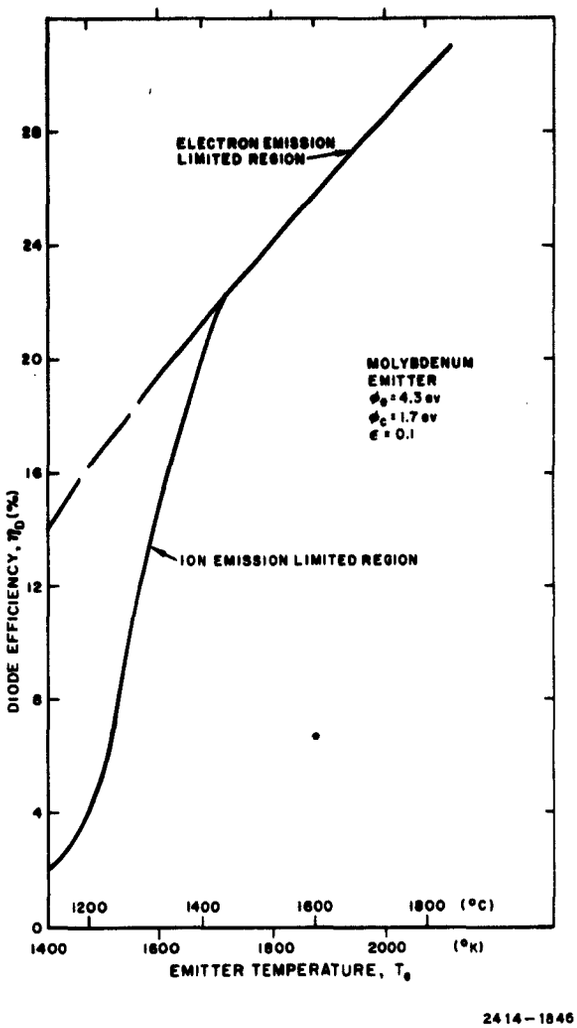

Figure 28. Emission-Limited Efficiencies for the Cesium Thermionic Converter

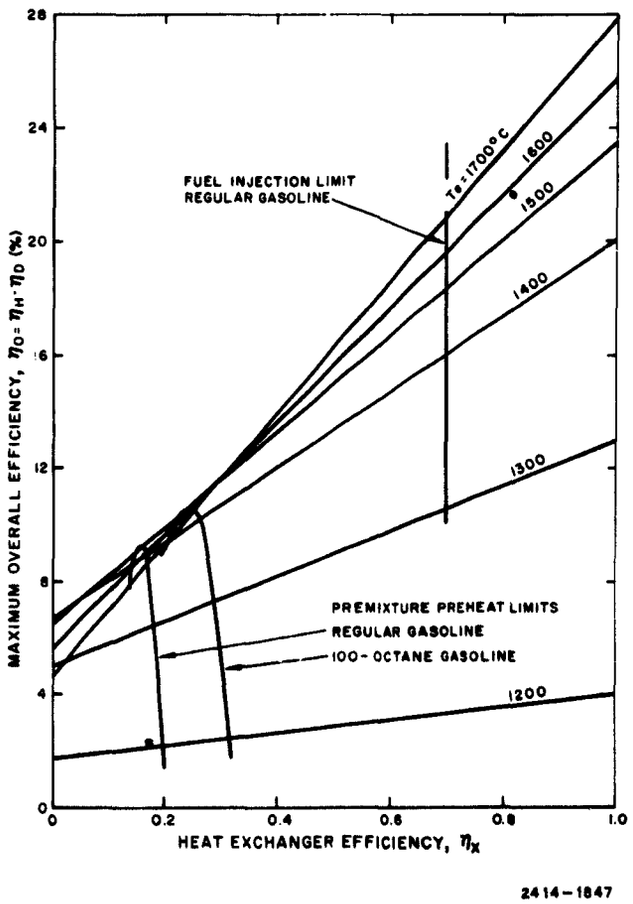

Figure 29. Maximum Overall Efficiencies for Flame-Heated Thermionic Converter Systems (Gasoline Fueled)

TABLE IX

MAXIMUM HEAT EXCHANGER EFFICIENCY WITH CONTINUOUS FUEL INJECTION (T_e = 1500°C)

Fuel	Maximum η_X
Methane	0.85
Propane	0.87
Regular Gasoline	0.70

close one can approach the maximum heat exchanger efficiency, shown in Table IX, depends upon the number of transfer units that can be built into a heat exchanger without exceeding a reasonable air supply pressure.

Theoretical Overall Efficiency

The heating efficiencies can now be combined with the corresponding values of the theoretical diode efficiency, η_D, to show the potential overal efficiencies, η_O, of a flame-heated thermionic converter system. Figure 28 shows the η_D's for a molybdenum emitter, as reported by Rasor and Weeks. Figure 29 shows the maximum overall efficiencies for gasoline-heated thermionic converter systems as a function of emitter temperature and heat exchanger efficiency. For perfect heat economy (i.e., $\eta_X = 1.0$), $\eta_O = \eta_D$, and η_O is seen to increase with increasing T_e. For lower values of η_X, the maximum overall efficiency (η_O) may correspond to lower emitter temperatures. Figure 29 indicates that the most efficient T_e for $\eta_X < 0.05$ would be 1400°C. The T_e = 1500°C system is seen to be the most efficient in the $0.05 < \eta_X < 0.3$ range, and coincides with the known preheat limitations for both gasolines. Figure 29 also shows that, for systems using premixed gasoline and air, there is little η_O penalty in operating at T_e = 1400°C, rather than at the slightly more efficient 1500°C. The lower temperature would be much more favorable, from the emitter corrosion standpoint. Notice that, for a premixed gasoline-air diode heater, the limit on overall efficiency (η_O) is 11%.

For gasoline fuel injection, however, there is no optimum temperature, from a theoretical standpoint (See Figure 29). Note that, at T_e = 1700°C, the maximum η_O = 21%.

It should be emphasized that Figure 29 is computed, using limiting values for both heat transfer and diode efficiency, and therefore operating flame-heated diodes would have a considerably smaller efficiency.

Heat Exchange Limitations

Once the heat leak is reduced to a minimum by proper design, which means placing the diode heater inside the diode, the next concern is to design an efficient heat exchanger. The design of the heat exchanger is governed by the available air supply pressure. The higher the available air supply pressure, the more compact the heat exchanger can become, for the same duty. In the previous section, consideration of thermodynamic principles revealed the limitations on heating efficiency for the case when: (1) the air-fuel mixtures were preheated, and (2) when the air was preheated and the fuel was injected at the maximum allowable temperature. These limitations are based upon a hypothetical heat exchanger, in which heat is transferred by an infinitesimally small driving force, ΔT_X. Now we will consider how close to the limit it is worthwhile to operate. The results of analysis for the case of regular gasoline and no insulation loss is presented in Figure 30. This figure shows the number of transfer units that are needed in the heat exchanger to obtain a given heat exchanger efficiency. A transfer unit is defined by the equation:

$$N_{Tu} = U A_X / w C_p$$

where

N_{Tu} = number of transfer units
U = heat transfer coefficient (w/cm^2-°C)
A_X = heat transfer area (cm^2)
w = flowrate (g/sec)
C_p = heat capacity at constant pressure (joules/g-°C)

Since N_{Tu} is dimensionless, any self-consistent set of units can be used. The N_{Tu} is not an extensive property of the heat exchanger, as is the heat transfer area or the size; but, for a given service, it is a convenient performance indicator, by which alternate heat exchanger designs can be compared. For example,

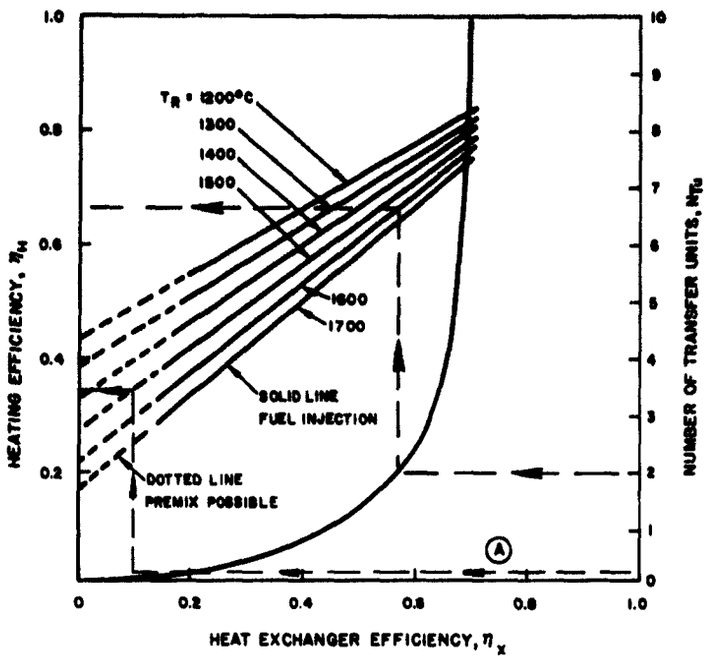

Figure 30. Design Chart for Regular Gasoline Fueled Diode Heaters ($Q_I = 0$)

the heat exchanger shown in Figure 14 is estimated to have an N_{Tu} of 0.1 when it is employed with a heat input of 1300 w. Assume also, for purposes of this estimate, that the gas temperature leaving the combustion chamber is 100° hotter than the emitter, and that the emitter is at 1400°C. Using Figure 30, as shown by line A, the predicted heating efficiency for this case is 35%, based upon no insulation loss whatsoever. This percentage should be compared with Run DD-23, which had 18% heating efficiency at 1400°C emitter temperature. This analysis shows that our diode heaters have attained about half the practically possible heating efficiency for the heat exchanger now being employed.

For the more advanced case, when fuel injection is employed, it still appears that a heat exchanger having an N_{Tu} of 2 is as large as is practical. For a T_e of 1500°C and a T_R of 1600°C, an η_H of 0.66 is obtained. If the length of the heat exchanger is doubled, N_{Tu} becomes 4 and η_H becomes 0.73. For a T_R = 1600°C, as $N_{Tu} \rightarrow \infty$, $\eta_H \rightarrow 0.77$. All these heating efficiencies are predicated upon negligible heat losses through the insulation.

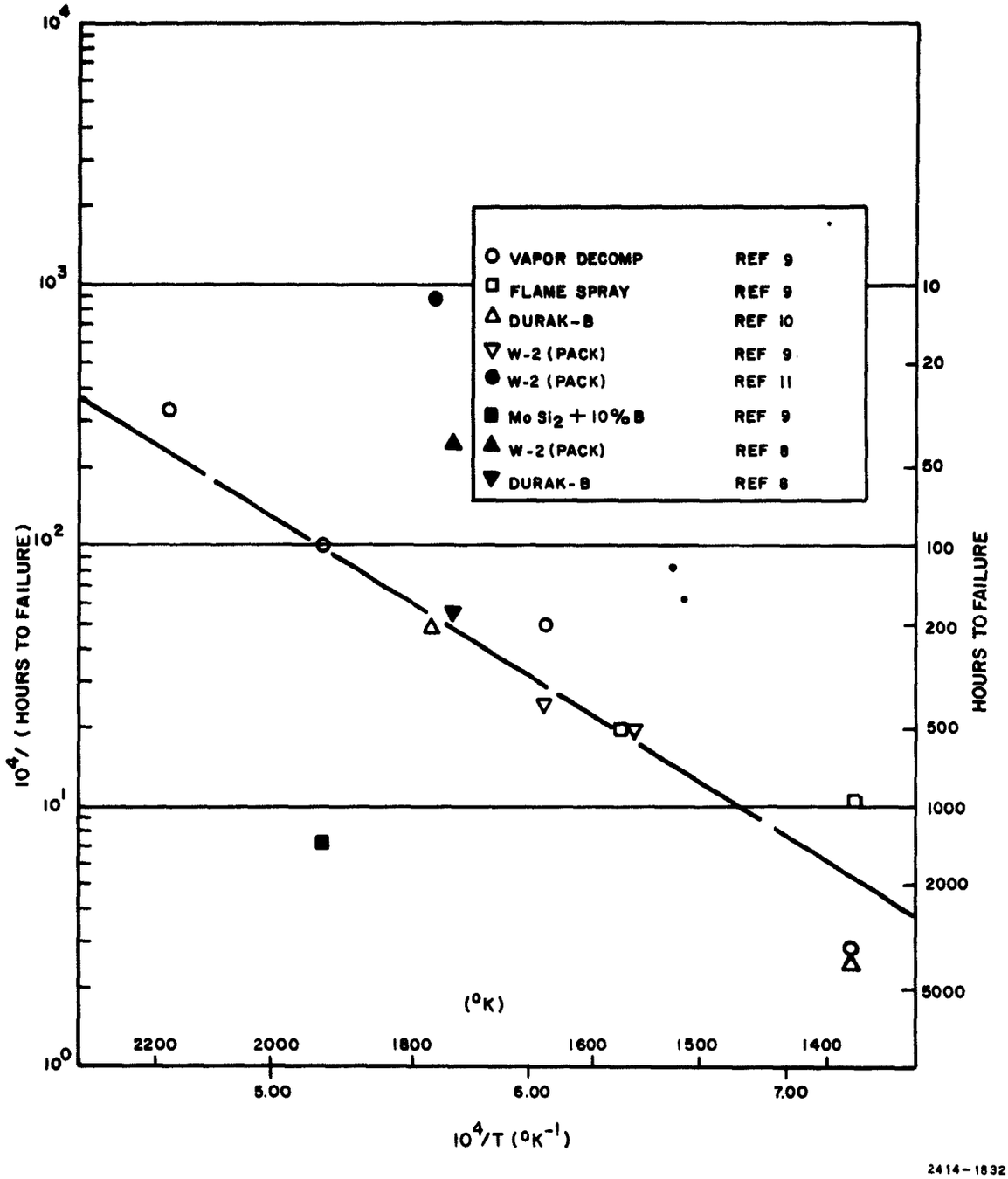

Figure 31. Protection Life of $MoSi_2$ Coatings, Exposure in Air

TASK C – MATERIALS DEVELOPMENT AND EVALUATION

Phase 1 – Protection of Molybdenum

Summary of Durak-B Data

The studies of the Durak-B protection coating on molybdenum have continued, as outlined in the earlier quarterly reports.[1,7] Since a number of tests of both 1.5-mil and 2.5-mil coatings have now been concluded, enough information has been accumulated to show that the Durak-B coating is superior to the other $MoSi_2$ coatings reported in the literature. This is illustrated by comparing the data shown on Figure 31 with those shown in Figures 32 and 33. Figure 31 is a summary of the published data on the protection lives afforded molybdenum by various $MoSi_2$ coatings. Because of the scarcity of the data and the lack of a definitive characterization of many of the coatings, the individual points are plotted without differentiation. In general, the coatings ranged from 1 to 3 mils in thickness, but the nominal coating thickness is a less important factor than is the uniformity of the coating and the absence of imperfections. The data shown in Figure 31 follow a reaction-rate trend (i.e., there is a suggestion that a straight line "fits" the data, when plotted as reciprocal hours to failure vs $°K^{-1}$). This curve suggests the service life should be about 100 hr at 2000°K, and about 500 hr at 1600°K.

The experimental data obtained during the report period are shown in Table X. Figure 32 summarizes all of the protection-life data obtained for air exposures of the Durak-B coating. The data shown with a line joining one of the legend symbols and an X represent runs in which the center portion of the wire sample was held at the test temperature, but the failure occurred at a lower temperature point. The X's locate the estimated temperatures of the failure points, and have a ±50°C uncertainty. The diagonal line shows the average of the published values of the protection lives of $MoSi_2$ coatings from Figure 31. The 1.5-mil Durak-B data are seen to fall above the line, indicating poorer protection. However, all but one of these samples failed at a temperature below the planned test temperature. The 2.5-mil Durak-B data, on the other hand, show better protection lives than the "average" curve. Since the thinner Durak-B coating is obviously poorer, our future work will involve only the 2.5-mil, and some 4-mil, coated samples now being prepared.

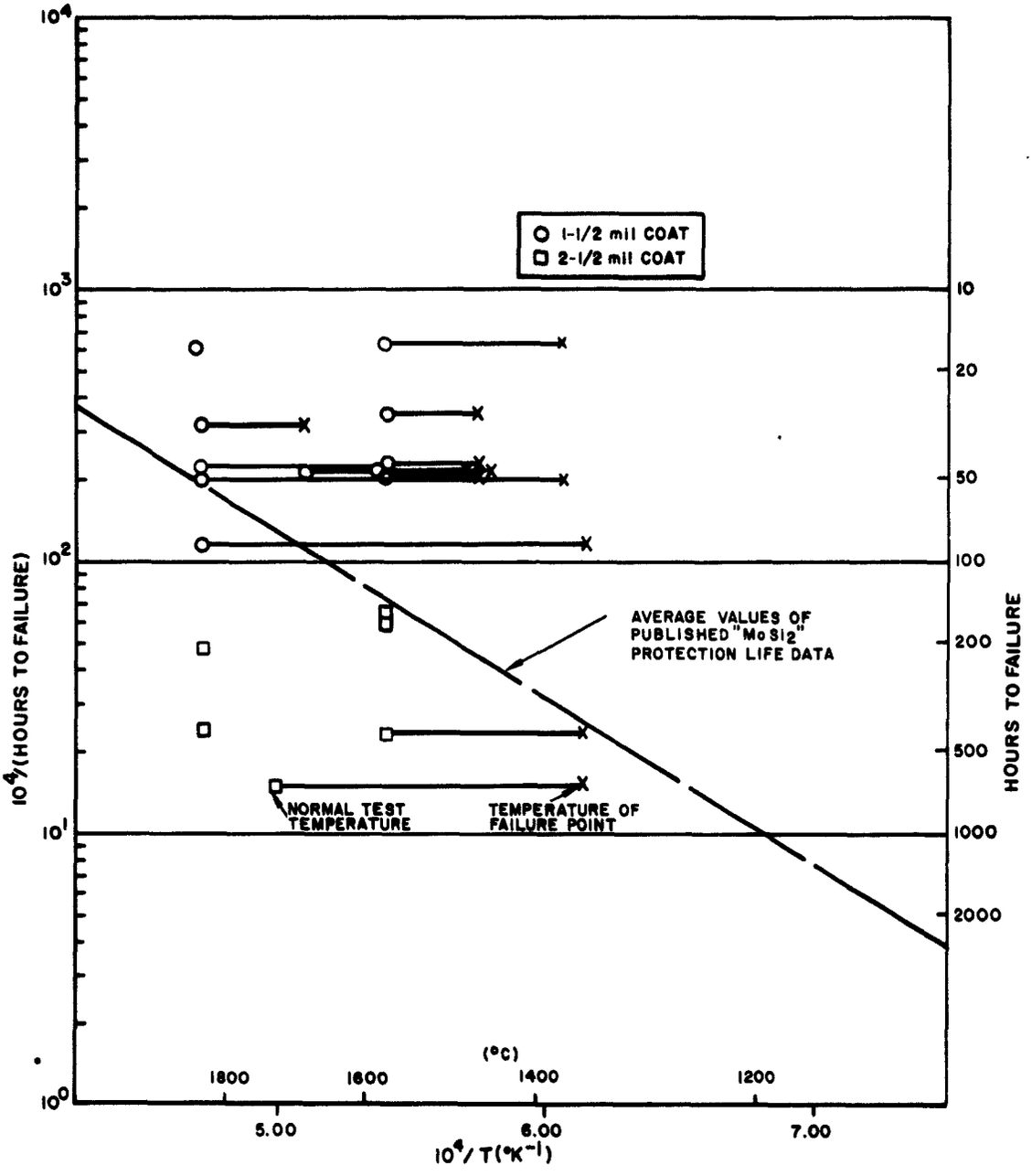

Figure 32. Protection Life of Durak-B Coatings, Exposure in Air

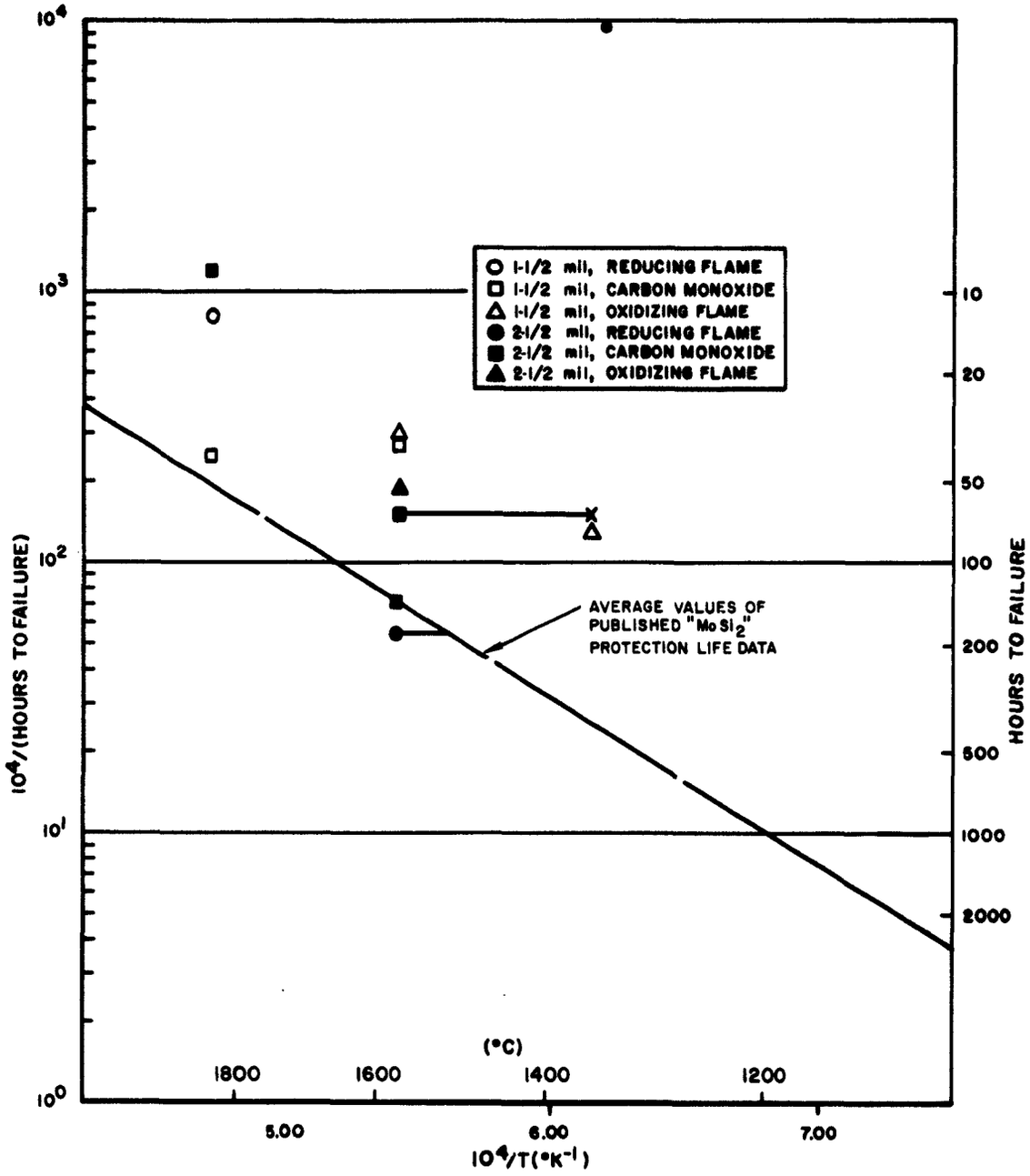

Figure 33. Protection Life of Durak-B Coatings in Flame Components

TABLE X

SUMMARY OF CORROSION EXPERIMENTS ON DURAK-B COATED MOLYBDENUM SAMPLES

Sample Number	Nominal Coat (in.)	Test Environment	Nominal Temp. (°C)	Corrected Temp.* (°C)	Time (hr)	Notes	Remarks
365	0.0015	Air	1750	1840	12	1	Failed at center
370	0.0015	CO	1500	1570	35	2	Failed at center
371	0.0015	Ox. Flame	1500	1570	34	2	Failed at center
372	0.0015	Red. Flame	1750	1840	12	4	Failed at center
373	0.0015	Ox. Flame	1300	1350	77+	2	Test terminated by a general power failure
375	0.0015	CO	1750	1840	41	3	Failed at center
391	0.0025	Air	1650	1730	262	1	Failed at center
392	0.0025	Air	1750	1840	20	1	Failed at center
393	0.0025	Air	1500	1570	151	1	Failed at quarter-point
399	0.0025	CO	1500	1570	68	2	Failed near end
400	0.0025	Ox. Flame	1500	1570	54	2	Failed at center
801	0.0025	Air	1500	1570	155	4	Failed at center
802	0.0025	Air	1500	1570	168+	4	Test terminated by a general power failure
803	0.0025	Red. Flame	1750	1840	8	4	Failed at the edge of the flame
804	0.0025	Air	1300	1350	670	4	Failed 1/2 in. from center
806	0.0025	Air	1300	1350	432	4	Failed near end
810	0.0025	CO	1500	1570	181	4	Failed at center

*Temperature corrected for an assumed emissivity of 0.6

Notes

1 Na-Ca glass wash over entire sample
2 Pre-oxidized at 1300°C in air
3 Pre-oxidized at 1500°C in air
4 No pre-oxidation

Supplemental Protection With a Glaze

Although the reason for the low-temperature (1300 to 1400°C) failure is not known, it has been postulated that the silica-cristobalite transition may be the cause.[1, 7, 12] This transition converts the glassy silica phase to the crystalline cristobalite, which might well be a poorer protection agent. A suggested technique for inhibiting the transition is to coat the Durak-B coating with a thin low-melting glass, with the expectation that the SiO_2 produced by the oxidation of the $MoSi_2$ will combine with the glass. The mixture would also be low-melting; and, if a proper combination were found, the final glassy phase would operate near its melting point. Hopefully, the tendency for cristobalite to crystallize out would be materially reduced. The first glass chosen for this study is a soda-lime glass, made from chemically pure components and fused at 1350°C. The initial composition is 11.0 mol % Na_2O, 10.5 mol % CaO, and 78.5 mol % SiO_2; and its melting point is 1300°C. This glass has been used to cover both 1.5-mil and 2.5-mil Durak-B coated molybdenum wires. It was found that completely covered samples were superior to the partially covered samples. The coating appears to be solving the problem of low-temperature failures, but uniformly long protection lives have not yet been observed. Additional tests are planned.

Protection From Flame Components

In addition to these studies of supplemental glass protection, a series of tests of the Durak-B coating in flame components has begun. Since even grossly oxidizing flames have localized regions which have reducing species; and since the SiO_2 glass, which is the protection agent formed in the oxidation of the $MoSi_2$ (Durak-B) coatings, is known to be susceptible to chemical reduction;[12] one expects the service life of these coatings to be shorter in flames than in air. Figure 33 shows the results obtained. As expected, the service lives are lower than those shown for air exposures on Figure 31. Although there seems to be a less clear-cut separation between the 1.5-mil and 2.5-mil sample data, there are too few samples, at present, to warrant a firm conclusion.

Metallographic Examination

In addition to these observations on the behavior of the glassy protection layer, microscopic examinations of the protective layer in exposed samples lead to some tentative conclusions about the migration of the silicon. When the Durak-B coating is applied, the silicon reacts with the surface molybdenum and

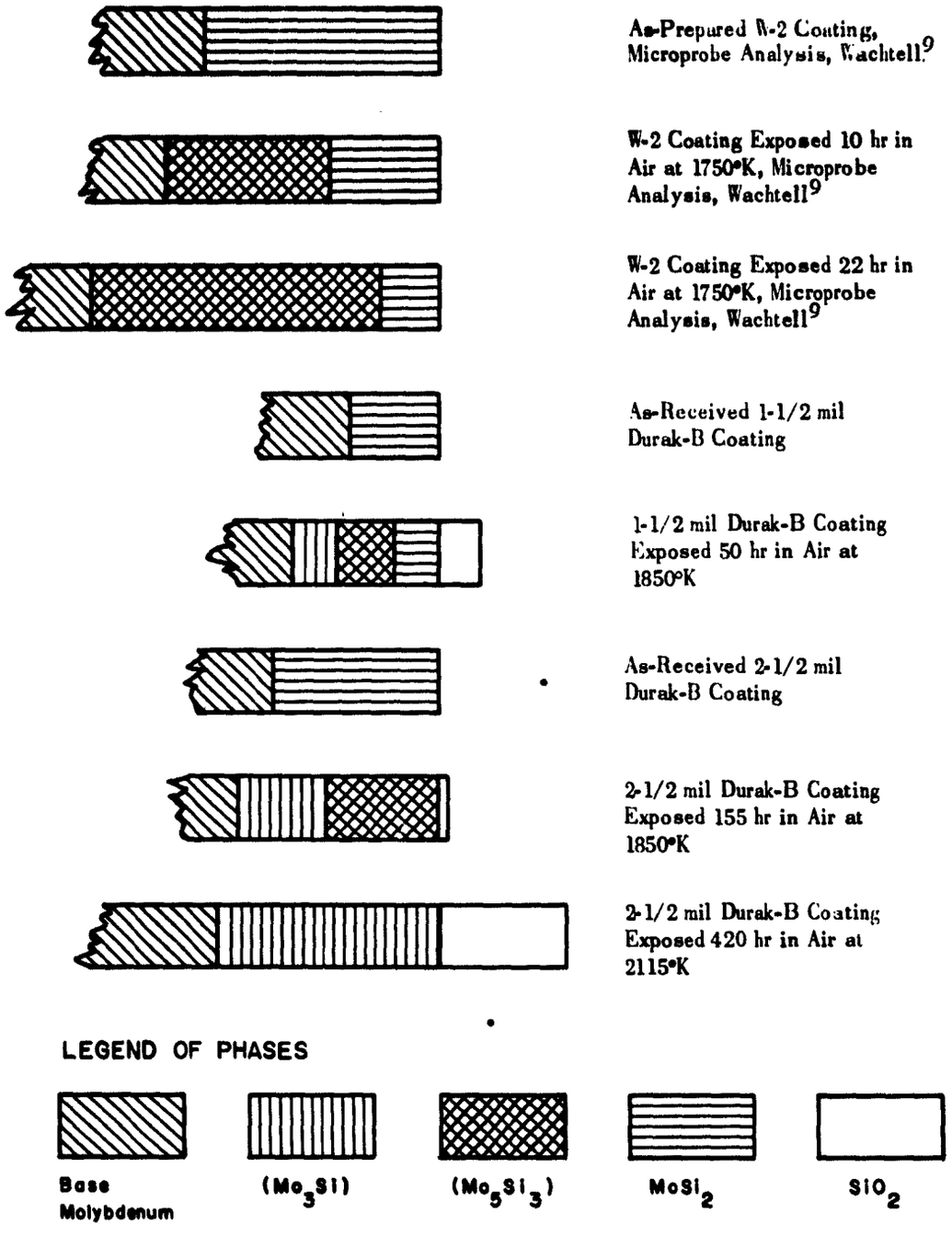

Figure 34. Summary of $MoSi_2$ Coating Behavior After Air Exposures

forms the disilicide. As the specimens are heated, the silicon tends to diffuse inward. After a few hours at 1570°C, a new phase appears beneath the $MoSi_2$. This is also noted by Wachtell,[8] who used an electron microprobe technique for analysis. A summary of his data is shown in Figure 34, together with a summary based upon microscopic examinations of our exposed Durak-B samples. This second phase appears as columnar crystals, using our present etching technique (Conc. HNO_3 etch for 3 to 5 sec, followed by a 1:1 HCl rinse, and then by a distilled water rinse). The composition of this phase is presumably the compound Mo_5Si_3. Upon further heating, a third intermetallic phase appears between the Mo_5Si_3 and the base Mo. This is tentatively assigned the composition Mo_3Si. No additional phases appear. Figure 34 shows this sequence in schematic form. At 1850°K (1570°C), the "Mo_5Si_3" phase begins to form during the first 10 hr of exposure; and the "Mo_3Si" phase appears after, say, 30 hr. After 155 hr at 1850°K, even a 2-1/2-mil $MoSi_2$ coating has virtually disappeared, and the "Mo_5Si_3" and the "Mo_3Si" layers are both prominent. At higher temperatures, the diffusion rate of the silicon is increased; so that, after about 200 hr at 2115°K (1840°C), only the "Mo_3Si" layer remains. Figure 34 shows the conditions resulting from a 420-hr exposure at 2115°K (1840°C) of a 2-1/2-mil Durak-B coated sample. An examination of the hardness profiles of the samples suggests that there is little tendency for silicon to diffuse into the base molybdenum until an appreciable amout of "Mo_3Si" has been formed. This conclusion is based upon the fact that the hardness profiles of the samples showing no "Mo_3Si", or only small amounts of "Mo_3Si," are uniform through the molybdenum core. In samples having a thick "Mo_3Si" layer, the hardness profile shows a decreasing hardness, as one moves inward from the Mo-"Mo_3Si" interface. The difference between the interface hardness value and the centerline hardness value, and the thickness of the diffusion shell, are functions of the exposure time. It therefore appears that, in addition to the external corrosive agents which tend to attack the SiO_2 glass and remove silicon by evaporation, there is an active "internal" mechanism which removes the silicon from the protection medium by inward diffusion. Both of these mechanisms contribute to the gradual loss of silicon from the protection coat, and eventually lead to failure. Nevertheless, the estimated lifetimes at, say, 1700°C approach a thousand hours, even in flame components.[12]

TABLE XI

SUMMARY OF SiC TESTS

Sample Number	Material*	Test Duration (hr)	Nominal Test Temp. (°C)	Corrosion Rate (mg/hr-cm^2)	Remarks
818	D1552	7	1575±	- 3.4	Sample rather badly corroded
821A†	D1552	4.5	1350	+ 0.64	Sample normally oxidized
821B†	D1552	5	1400	+ 0.45	Sample normally oxidized
821C†	D1552	6	1100	+ 0.2	Sample normally oxidized
824	3330	1	1700	-93.	Sample very badly corroded
826	2827	6.8	1575	+ 3.65	Sample normally oxidized
832	A978	5	1600	- 8.05	Sample rather badly corroded
201	KT	5	1800+	---	1/8-in. rod sample demolished
202	KT	7	1700	- 1.68	1/8-in. rod sample normally oxidized
207	KT	6.5	1600	+ 2.35	1/4-in. rod sample normally oxidized
208	KT	5	1750	-16.	1/4-in. rod rather badly corroded
209	KT	7	1750±	-10.6	1/4-in. rod rather badly corroded

*These materials were provided by the Carborundum Co. D1552 is a low-temperature "Carbofrax" mixture; 3330 is a special "Refrax" mixture; 2827 is a "Refrax" mixture; A978 is a high-temperature "Carbofrax" mixture; and KT is their special high-density silicon-impregnated material.
† Samples labelled A,B, and C were run sequentially.

Phase 2 – Corrosion of Silicon Carbide

Because we are contemplating the use of a silicon carbide cup as an auxiliary flame barrier, a number of silicon carbide samples have been exposed in our brick propane-fired furnace. The furnace is described in an earlier report.[1] Table XI summarizes the tests. Examination of the data clearly indicates that the KT silicon carbide is superior to the other varieties tested. The maximum service temperature of 1700°C, indicated by these tests, is in good agreement with that reported by T. H. Elmer.[13]

Phase 3 – Gas Permeation

The study of the permeation of flame components through a molybdenum shell has begun. Until quite recently, we have been unable to prepare adequate molybdenum-to-molybdenum welds, and a suitable capsule could not be fabricated. During this report period, a suitable welding technique was found (described in detail under Task C, Phase 4), and two capsules have been prepared. The capsules are made by welding 1/4-in. end-pieces to a 0.010-in. wall, 3/4-in. diameter tube. The upper end-piece has a 1/4-in. rod welded to it. This rod is step-drilled, to make a lead-tube through which the gases will be removed for analysis. The effective area of the permeation cell is $0.75\pi(0.839) = 1.98\,in^2$, or $12.8\,cm^2$. These capsules have been sent to the Chromizing Corp. of Hawthorne, California, for application of a 2-1/2-mil Durak-B coating. The capsules are scheduled to be completed in mid-April. It is planned to use our small pebble-bed furnace as the source of heat and of flame components. One of the capsules will have a silicon carbide cup as an auxiliary flame protector, to simulate the proposed thermionic diode system. If the permeation of this system is negligibly small, the second capsule will be tested without the cup.

Phase 4 – Welding of Molybdenum

There are many references to welding molybdenum, which largely agree on the following observations:

1) Tungsten-inert-gas welding leaves a wide heat-affected zone with large grain size

2) Metal impurities (particularly oxygen and nitrogen) seriously impair the weldability

3) Very little is really known about the welding process, and good joints are largely a matter of art

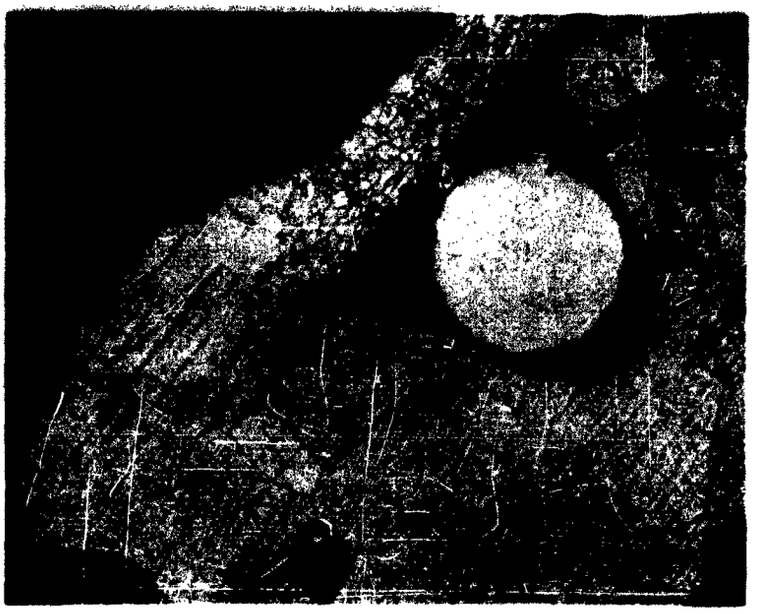

2414-1858

Figure 35. Photomicrograph of Successful Mo-Mo End Cap Weld

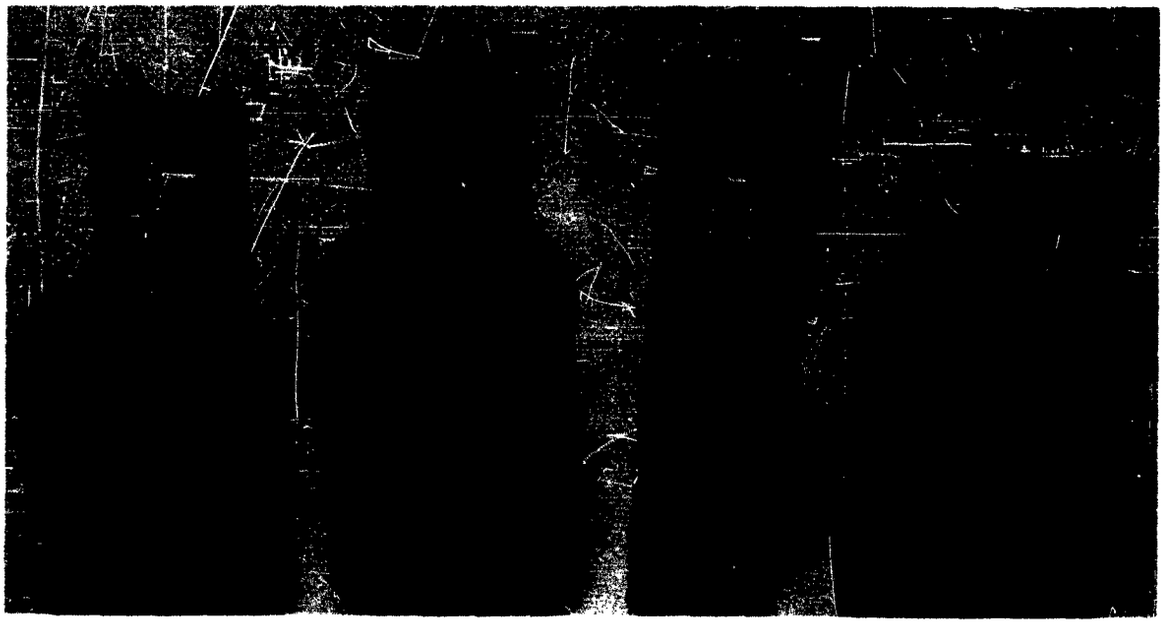

2414-1866 A

Figure 36. Mo-to-Mo Welds

Early results with retort welds, in this laboratory, were disappointing. Cracks formed on aging, and the joints were exceedingly brittle. Thin sections also warped badly. However, recently, a type of Mo-Mo end cap weld has been developed with moderate success. Figure 35 shows a photomicrograph of such a joint. Note that the heavy arc-cast end cap is made to melt and flow over the thin drawn tube. The fine grain structure of the thin tube is retained for flexibility. The end cap retains its large grain size, which is not detrimental because no flexing is required.

Figure 36 shows the external appearance of several such weldments, successively modified to require less heat for welding. This welding technique was used to fabricate the capsules for the gas permeation study.

CONCLUSIONS

1. Sapphire spacers were successfully used to maintain emitter-collector spacing.
2. Failure of alumina seals is a serious problem, and more attention should be paid to it.
3. A heater for the demonstration diode, capable of attaining thermionic temperature and heat flux, has been demonstrated.
4. Although diode heaters using premixed air and fuel work well, more efficient heat exchangers and fuel injection are required, if high overall efficiencies are to be attained.
5. Thick Durak-B is still the best primary protective coating for molybdenum.

PROGRAM FOR NEXT QUARTER

TASK A – DIODE DEVELOPMENT

The four demonstration diodes will be completed and tested. Possible experiments with the flame-heated diodes are:

1) Diode characteristics, including optimum operation efficiency vs emitter temperature curve
2) 60 cps volt-ampere curves
3) Series-connected diode tests
4) Diode life testing

TASK B – HEAT SOURCE DEVELOPMENT

The present diode heater will be perfected, so that long-life operation can be achieved. Operation with gasoline fuel will be attempted. A portable test stand will be constructed, to demonstrate operation of the flame-heated diodes. Application of the demonstration type flame-heated diode to portable power sources will be investigated.

The problem of temperature control of the components will be investigated further.

TASK C – MATERIALS DEVELOPMENT

Evaluation of coatings for molybdenum will continue; the use of protective glazes on the outside, and diffusion barriers within, will be tried.

An experiment will be completed to measure the permeability of Durak-B coated molybdenum to gases from a flame. This permeability is to be measured at a number of temperatures.

TASK D – ELECTRICAL DEVELOPMENT

The triggered diode concept for power conversion will be analyzed further; and, if warranted, two flame-heated diodes may be operated in a triggered diode circuit.

KEY PERSONNEL ASSIGNED TO PROJECT

		Hours Worked During Third Quarter
D. H. Adair	Sr. Mechanic	510.1
E. V. Clark	Research Engineer	414
R. G. Cole	Mechanic-Engineering Laboratory, Junior	314.1
W. R. Martini	Project Engineer	500
R. L. McKisson	Project Engineer and Supervisor	232.5

NOMENCLATURE

A_X = Area of heat exchanger surface (cm^2)

C_p = Heat capacity at constant pressure (joules/g-°C)

N_{Tu} = Number of Transfer Units (dimensionless)

Q_A = Heat content of air stream (w)

Q_e = Heat entering the emitter (w)

Q_F = Heat (potential chemical energy of combustion) of the fuel entering system (w)

Q_I = Heat loss to surroundings (w)

Q_P = Heat transferred to the incoming gas stream (preheat) (w)

Q_R = Heat content of exhaust gas stream at the emitter temperature (w)

Q_S = Heat content of stack gas (w)

q_e = Heat flux (w/cm^2)

T_c = Collector temperature (°C)

T_{Cs} = Cesium reservoir temperature (°C)

T_e = Emitter temperature (°C)

T_R = Temperature of gases leaving combustion chamber (°C)

U = Overall heat transfer coefficient (w/cm^2-°C)

w = Gas flow rate (g/sec)

ΔT_X = Effective temperature difference across heat exchanger surfaces

ϵ = Thermal emissivity

η = Efficiency

η_D = Diode efficiency, (max. elec. power)/Q_e

η_H = Emitter heating efficiency, Q_e/Q_F

η_O = Overall system efficiency, $\eta_H \eta_D$

η_X = Heat exchanger efficiency, Q_P/Q_R

ϕ_c = Collector work function (ev)

ϕ_e = Emitter work function (ev)

REFERENCES

1. W. R. Martini and R. L. McKisson, "Flame Heated Thermionic Converter Research, Second Quarterly Report," AI-6981 (April 1962)

2. M. I. Jacobson and D. C. Martin, "Brazing Molybdenum for High-Temperature Service," The Welding Journal, 34 (1955) 65s-74s

3. W. R. Martini, "Design Considerations for Gasoline Powered Thermionic Generators," a paper to be presented at the 16th Annual Power Sources Conference, May 22-24, 1962, in Atlantic City, New Jersey

4. S. S. Kitrilakis and G. N. Hatsopoulos, "Recent Experimental Results in Thermionic Research at Thermo Electron Engineering Corporation," PIC-ELE-TI-209/1 (January 30, 1962)

5. J. H. Keenan and F. G. Keys, Thermodynamic Properties of Steam, (John Wiley and Sons, Inc., New York, 1944)

6. N. S. Rasor and C. C. Weeks, "First Summary Report: Thermionic Converters for Compact Nuclear Power Plants," NAA-SR-7144 (to be published)

7. W. R. Martini, R. L. McKisson, and R. G. Hoff, "Flame Heated Thermionic Converter Research, First Quarterly Report," AI-6815 (April 1962)

8. Wachtell, "Protective Coatings for Molybdenum," a paper given at the Ceramics and Composites, Coatings and Solid Bodies Symposium, Society of Aerospace Materials and Process Engineers Meeting, November 14-15, 1961, in Dayton, Ohio

9. E. S. Bartlett, H. R. Ogden, and R. I. Jaffee, DMIC Report 109 (ASTIA AD 210978; OTS PB 151064) (March 1959)

10. A. Fletcher, Chromizing Corp. Sales Engineer, private communication

11. W. D. Kloop, DMIC Memo 102 (April 1961)

12. R. L. McKisson, "Emitter Corrosion in Thermionic Converters," a paper to be presented at the Symposium on Thermionic Power Conversion, May 14-17, 1962, in Colorado Springs, Colorado

13. T. H. Elmer, "High Temperature Reactions in the System SiC-SiO_2," NEPA-1770 (1950)

AD

Atomics International, Canoga Park, Calif.

FLAME HEATED THERMIONIC CONVERTER RESEARCH

by W. R. Martini, R. L. McKisson, and E. V. Clark

3rd Quarterly Report, 1 Jan - 31 Mar 1962

74 pp, 36 illus., 13 refs.

(Report No. AI-7330)

(Contract DA 36-039 SC-88982

Unclassified Report

The purpose of this research is to develop the technology required for portable, flame-heated, thermionic power sources. Active development in thermionic diodes, heat sources, and materials is underway.

The 150 w(e) electrically heated diode developed a cesium leak in the seal insulator. However, before the cesium was exhausted, some data were obtained defining the necessary operating parameters for a triggered diode power inversion system.

Four flame-heated thermionic converters are being constructed

The heater for the above converters was tested. An emitter temperature of 1450°C was attained, along with a heat flux of 28 w/cm^2. An analysis of possible efficiencies for diode heaters emphasized that heaters employing fuel injection, in combination with a high efficiency heat exchanger, must eventually be developed

(over)

UNCLASSIFIED

1) Combustion Chambers

2) Combustion Chamber Liners

3) Molybdenum Compounds and Silicides

4) Silicon Compounds and Carbides

5) Inverter Rectifiers

6) Diodes (Electronic Tube Devices) – Cesium vapor

7) Power Supplies (Power Equipment)

I Thermionic Converter Research

II Martini, W. R.

III McKisson, R. L.

IV Clark, E. V.

V U.S. Army Signal Research & Development Laboratory, Ft. Monmouth, New Jersey

VI Contract No. DA 36-039 SC-88982

UNCLASSIFIED

AD

Atomics International, Canoga Park, Calif.

FLAME HEATED THERMIONIC CONVERTER RESEARCH

by W. R. Martini, R. L. McKisson, and E. V. Clark

3rd Quarterly Report, 1 Jan. - 31 Mar. 1962

74 pp, 36 illus., 13 refs.

(Report No. AI-7330)

(Contract DA 36-039 SC-88982

Unclassified Report

The purpose of this research is to develop the technology required for portable, flame-heated, thermionic power sources. Active development in thermionic diodes, heat sources, and materials is underway.

The 150 w(e) electrically heated diode developed a cesium leak in the seal insulator. However, before the cesium was exhausted, some data were obtained defining the necessary operating parameters for a triggered diode power inversion system.

Four flame-heated thermionic converters are being constructed.

The heater for the above converters was tested. An emitter temperature of 1450°C was attained, along with a heat flux of 28 w/cm^2. An analysis of possible efficiencies for diode heaters emphasized that heaters employing fuel injection, in combination with a high efficiency heat exchanger, must eventually be developed.

(over)

UNCLASSIFIED

1) Combustion Chambers

2) Combustion Chamber Liners

3) Molybdenum Compounds and Silicides

4) Silicon Compounds and Carbides

5) Inverter Rectifiers

6) Diodes (Electronic Tube Devices) – Cesium vapor

7) Power Supplies (Power Equipment)

I Thermionic Converter Research

II Martini, W. R.

III McKisson, R. L.

IV Clark, E. V.

V U.S. Army Signal Research & Development Laboratory, Ft. Monmouth, New Jersey

VI Contract No. DA 36-039 SC-88982

UNCLASSIFIED

AD

Testing of Durak-B coating for molybdenum metal continued. Analysis of results showed that the coating fails, due to depletion of silicon. Silicon may evaporate as SiO_2 or diffuse into the molybdenum metal.

Flame corrosion tests on silicon carbide refractories have shown the superiority of KT silicon carbide.

UNCLASSIFIED

UNITERMS

Thermionics

Converters

Diodes

Molybdenum

Molybdenum Disilicide

Protective Coatings

Combustion

Durak-B

Propane

Gasoline

Silicon Carbide

UNCLASSIFIED

AD

Testing of Durak-B coating for molybdenum metal continued. Analysis of results showed that the coating fails, due to depletion of silicon. Silicon may evaporate as SiO_2 or diffuse into the molybdenum metal.

Flame corrosion tests on silicon carbide refractories have shown the superiority of KT silicon carbide.

UNCLASSIFIED

UNITERMS

Thermionics

Converters

Diodes

Molybdenum

Molybdenum Disilicide

Protective Coatings

Combustion

Durak-B

Propane

Gasoline

Silicon Carbide

UNCLASSIFIED

DISTRIBUTION

	Copies
Deputy President U.S. Army Security Agency Board Arlington Hall Station Arlington 12, Virginia	(1)
Commander Armed Services Technical Information Agency ATTN: TIPCR Arlington Hall Station Arlington 12, Virginia	(10)
Chief U.S. Army Security Agency Arlington Hall Station Arlington 12, Virginia	(2)
Commander Aeronautical Systems Division ATTN: ASAPRL Wright-Patterson Air Force Base, Ohio	(1)
AFSC Liaison Office Naval Air Research and Development Activities Command Johnsville, Pennsylvania	(1)
Commander Air Force Cambridge Research Laboratories ATTN: CRO L. G. Hanscom Field Bedford, Massachusetts	(1)
Commander Air Force Command and Control Development Division ATTN: CCRR ATTN: CCSD L. G. Hanscom Field Bedford, Massachusetts	(1) (1)
Liaison Officer, LAA U.S.A. Signal Research and Development Laboratory 75 South Grand Ave., Bldg. 13 Pasadena, California	(1)
Power Information Center Moore School Building 200 South Thirty-Third Street Philadelphia 4, Pennsylvania	(1)
Deputy Commander, AFSC for Aerospace Systems, ATTN: Mr. W. J. Bennison Aerospace Library Air Force Unit Post Office Los Angeles 45, California	(1)
Army Research Office Office, Chief Research & Development Department of the Army Room 3D442, The Pentagon Washington 25, D.C. ATTN: Dr. Sidney J. Magram	(1)
Director Advanced Concepts Division Bureau of Ships (Code 350) Washington 25, D.C. ATTN: LCDR, Frank W. Anders	(1)
Office of Naval Research (Code 429) Department of the Navy Washington 25, D.C. ATTN: Mr. James R. Patton, Jr.	(1)
Headquarters USAF (AFRDR-AS) Washington 25, D.C. ATTN: Maj. William G. Alexander	(1)

DISTRIBUTION

Copies

Commander
Aeronautical Systems Division
Wright-Patterson Air Force
Base, Ohio
ATTN: Mr. George W. Sherman (1)

Assistant Director, Material Sciences
Advanced Research Projects Agency
The Pentagon, Room 3E153
Washington 25, D. C.
ATTN: Mr. Charles F. Yost (1)

Advanced Research Projects Agency
The Pentagon, Room 3E157
Washington 25, D. C.
ATTN: Dr. John H. Huth (1)

U.S. Atomic Energy Commission
Division of Reactor Development
Washington 25, D. C.
ATTN: Mr. G. Montgomery Anderson (1)

U.S. Atomic Energy Commission
Division of Reactor Development
Auxiliary Power Branch (SNAP)
Washington 25, D. C. (1)
ATTN: Lt. Col. George H. Ogburn, Jr.

National Aeronautics & Space
Administration
1520 H. Street, N. W.
Washington 25, D. C.
ATTN: Mr. David Novik (RPP) (1)

National Aeronautics & Space
Administration
1520 H. Street, N. W.
Washington 25, D. C.
ATTN: Mr. Walter C. Scott (1)

Equipment & Supplies Division
Office of Ordnance
Office, DODR&E
The Pentagon
Washington 25, D. C.
ATTN: Mr. G. B. Wareham (1)

Copies

Radio Corporation of America
RCA Laboratories
Princeton, New Jersey
ATTN: Dr. K. G. Hernquist (1)

The Marquardt Corporation (1)
16555 Saticoy Street
Van Nuys, California
ATTN: Mr. Richard Laubenstein

Thermo Electron Engineering Corp.
85 First Avenue
Waltham 54, Massachusetts
ATTN: Mr. F. J. Lyczko (1)

General Instrument Corporation
Thermoelectric Division
65 Gouverneur Street
Newark 4, New Jersey
ATTN: Mr. Melvin Barmat (1)

The Babcock & Wilcox Company
Atomic Energy Division
1201 Kemper Street
P. O. Box 1260
Lynchburg, Virginia
ATTN: Mr. Paul F. Schutt (1)

General Electric Co.
Monmouth District Office
43 West Front Street
Red Bank, New Jersey
ATTN: Mr. Dexter Marcum (1)

Westinghouse Electric Corp.
43 West Front Street
Red Bank, New Jersey
ATTN: Mr. C. M. Arthur (1)

Ford Instrument Co.
Div. of Sperry Rand Corp.
31-10 Thomson Avenue
Long Island City 1, N. Y.
ATTN: Mr. T. Jarvis (1)

DISTRIBUTION

	Copies
The Bendix Corp. Red Bank Division Eatontown, N. J. ATTN: Mr. Joseph E. Sidoti	(1)
General Dynamic Corp. General Atomic Division 10955 John Jay Hopkins Drive San Diego 21, California	(1)
Library	(26)